THE JOURNAL OF PHYSICAL CHEMISTRY B
A JOURNAL OF THE AMERICAN CHEMICAL SOCIETY

pubs.acs.org/JPCB Article

Long-Lived Charge-Separated State in Naphthalimide−Phenothiazine Compact Electron Donor−Acceptor Dyads: Effect of Molecular Conformation Restriction and Solvent Polarity

Xiao Xiao,[▽] Yuxin Yan,[▽] Andrey A. Sukhanov,[▽] Sandra Doria,[▽] Alessandro Iagatti, Laura Bussotti, Jianzhang Zhao,* Mariangela Di Donato,* and Violeta K. Voronkova*

Cite This: https://doi.org/10.1021/acs.jpcb.3c02595 Read Online

ABSTRACT: To study the charge separation (CS) and long-lived CS state, we prepared a series of dyads based on naphthalimide (NI, electron acceptor) and phenothiazine (PTZ, electron donor), with an intervening phenyl linker attached on the N-position of both moieties. The purpose is to exploit the electron spin control effect to prolong the CS-state lifetime by formation of the ^{3}CS state, instead of the ordinary ^{1}CS state, the spin-correlated radical pair (SCRP), or the free ion pairs. The electronic coupling magnitude is tuned by conformational restriction exerted by the methyl groups on the phenyl linker. Differently from the previously reported NI-PTZ analogues containing long and flexible linkers, we observed a significant CS emission band centered at ca. 600 nm and thermally activated delayed fluorescence (TADF) with a lifetime of 13.8 ns (population ratio: 42%)/321.6 μs (56%). Nanosecond transient absorption spectroscopy indicates that in cyclohexane (CHX), only the ^{3}NI* state was observed (lifetime τ = 274.7 μs), in acetonitrile (ACN), only the CS state was observed (τ = 1.4 μs), whereas in a solvent with intermediate polarity, such as toluene (TOL), both the ^{3}NI* (shorter-lived) and the CS states were observed. Observation of the long-lived CS state in ACN, yet lack of TADF, confirms the spin-vibronic coupling theoretical model of TADF. Femtosecond transient absorption spectroscopy indicates that charge separation occurs in both nonpolar and polar solvents, with time constants ranging from less than 1 ps in ACN to ca. 60 ps in CHX. Time-resolved electron paramagnetic resonance (TREPR) spectra indicate the existence of the ^{3}NI* and CS states for the dyads upon photoexcitation. The electron spin−spin dipole interaction magnitude of the radical anion and cation of the CS state is intermediate between that of a typical SCRP and a ^{3}CS state, suggesting that the long CS-state lifetime is partially due to the electron spin control effect.

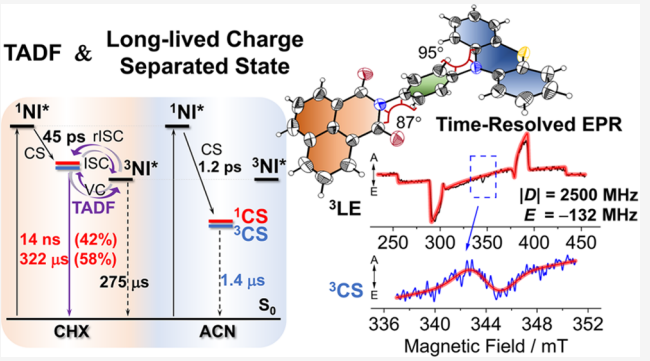

1. INTRODUCTION

Formation of long-lived charge separation (CS) states in organic electron donor−acceptor dyads/triads is crucial for fundamental photochemistry studies, as well as for artificial photosynthesis,[1−5] photocatalysis,[6−8] and photovoltaics.[9−15] Marcus theory can be used for describing the relation between the kinetics and thermodynamics of electron transfer (ET; eq 1)[16]

$$k_{ET} = \left(\frac{4\pi^3}{h^2\lambda k_B T}\right)^{1/2} V^2 \exp\left[-\frac{(\Delta G^0_{ET} + \lambda)^2}{4\lambda k_B T}\right] \quad (1)$$

where h and k_B represent the Planck constant and Boltzmann constant, respectively. ΔG^0_{ET} is the Gibbs free energy change between the equilibrium reactant and final states of the electron transfer, λ is the total reorganization energy, and the magnitude of the electronic coupling matrix element V indicates the coupling strength between the initial and the final states of the electron transfer.

As indicated by the Marcus theory of electron transfer (eq 1), a few approaches have been developed to prolong the CS-state lifetime. One method is to reduce the electronic coupling strength (V) between the initial state and the final CS state. In this case, one can use a long, rigid, saturated linker or multiple donors or acceptors, inducing cascade charge transfer (CT) processes.[17−19] The drawback of this method is the low energy of the final CS state (i.e., large energy loss during the generation

Received: April 19, 2023
Revised: July 3, 2023

Scheme 1. Synthesis of Compounds[a]

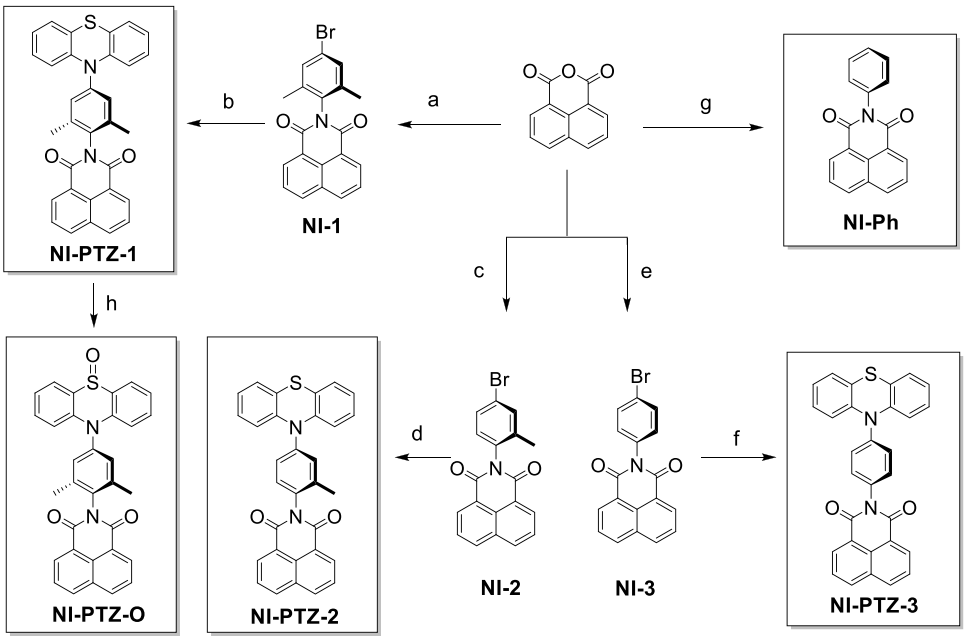

[a](a) 4-Bromo-2,6-dimethylaniline, acetic acid, N_2, reflux, 24 h, yield: 46%. (b) Phenothiazine, $Pd(OAc)_2$, K_2CO_3, $(t\text{-}Bu)_3PHBF_4$, toluene (TOL), N_2, reflux, 3 h, yield: 84%. (c) 4-Bromo-2-methylaniline, acetic acid, N_2, reflux, 24 h, yield: 36%. (d) Similar to step (a), yield: 59%. (e) 4-Bromoaniline, acetic acid, N_2, reflux, 6 h, yield: 34%. (f) Similar to step (a), yield: 95%. (g) Aniline, acetic acid, N_2, reflux, 6 h, yield: 64%. (h) H_2O_2 (30%), acetic acid, 50 °C, 2 h, yield: 19%.

of the CS state upon photoexcitation of the dyad, which is undesired) and the synthetic difficulties of the molecular systems containing long, rigid linkers. Alternatively, the Marcus inverted region effect was also used to prolong the CS-state lifetimes when $-\Delta G^0_{ET} > \lambda$, especially in systems presenting CS states with high energy and a small reorganization energy (λ), the lifetime of the CS state is generally long.[16,20,21]

A less used methodology is to use the electron spin control, i.e., to attain a triplet precursor (^{3}LE; LE: localized excited state) to initiate CS: since the electron transfer process is electron spin selective, the resulting CS state will also be a triplet, and a longer lifetime will be granted by the electron spin-forbidden nature of the charge recombination (CR) from the ^{3}CS state toward the ground state (S_0 state).[3,22−26] However, this strategy is difficult to be implemented in the case of conventional electron donor−acceptor dyads presenting large separation between the donor and the acceptor because often the electron exchange energy (J) between the radical anion and cation of the final CS state is too small to form stable ^{3}CS states. In these cases, very often a spin-correlated radical pair (SCRP) is formed, if not an ion pair without any spin−spin dipolar interaction between the radical anion and the radical cation.[27,28] Strong spin−spin dipolar interactions between the radical anion and the radical cation of a CS state require a short distance between the two; thus, compact electron donor−acceptor dyads are desired to access the long-lived ^{3}CS states, but these dyads were rarely reported.[3] The short distance between the radical anion and cation may lead to strong electronic coupling and accelerate both the CS and CR, shortening the CS-state lifetime. On the other hand, a triplet precursor for CS is difficult to access in heavy atom-free dyads because of poor intersystem crossing (ISC) to produce such a state. In some cases, however, the CS-state lifetime can be prolonged through a spin control effect. For instance, in a fully conjugated phthalocyanine-perylenebenzimidazole dyad, the lifetime of the CS state was determined as 0.26 ms.[25] Since the precursor of the CS state is the ^{3}ZnPc* state, the CS state might also be a triplet: this example demonstrates that the electron spin control effect may contribute to prolong the CS-state lifetime. In another similar tetrad with phenothiazine (PTZ) as the electron donor, a nitrophenyl unit was used as the electron acceptor and a N^N Pt(II) bisacetylide complex as the linker (also chromophore to produce the ^{3}MLCT state as the precursor for CS), and a CS state with a lifetime of ca. 70 ns was observed in dichloromethane (DCM) or dimethylformamide (DMF).[29] Further increasing the distance and reducing the coupling between the PTZ donor and the nitrophenyl acceptor in the Pt(II) acetylide complex prolongs the CS lifetime to ca. 230 ns.[30] However, the complicated molecular structure makes the synthesis of the related compounds challenging.

Furthermore, an interesting scenario occurs if the π-conjugation planes of the electron donor and acceptor units adopt an orthogonal geometry and the energies of the ^{3}LE and ^{3}CS states are similar. In this case, thermally activated delayed fluorescence (TADF) can be observed.[31−39] TADF materials are not only important in fundamental photochemistry studies but also for applications in organic light-emitting diode (OLED) materials[40−42] or triplet−triplet annihilation (TTA) upconversion.[43−47] However, detailed photophysical mechanisms of electron donor−acceptor TADF emitters are still not fully revealed. Although it was recently proposed that a two-state model (only ^{1}CS and ^{3}CS or ^{3}LE states are considered) is not sufficient to rationalize the TADF, in-depth investigations of the TADF mechanism are rare.[48−51]

In order to tackle the above challenges, herein, we prepared a series of compact electron donor−acceptor dyads, with 1,8-naphthalimide (NI) as the electron acceptor and phenothiazine (PTZ) as the electron donor. The two units are connected by a 1,4-phenylene linker attached on N-positions of both

https://doi.org/10.1021/acs.jpcb.3c02595
J. Phys. Chem. B XXXX, XXX, XXX−XXX

chromophores (Scheme 1). Moreover, to tune the electron coupling magnitude between the electron donor and acceptor, two, one, or no methyl groups are attached on the phenylene linker in **NI-PTZ-1**, **NI-PTZ-2**, and **NI-PTZ-3**, respectively. One of the advantages of the current rigid dyads is the well-defined distance and mutual orientation between the electron donor and acceptor, reducing conformational fluctuations in fluid solutions. It should be pointed out that the electron spin−spin exchange and dipolar interaction between the radical anion and cation of the CS state may lead to the formation of the ^{1}CS/^{3}CS state, instead of the SCRP or free ion pairs. Based on **NI-PTZ-1**, **NI-PTZ-O** was prepared, in which the sulfur of the PTZ unit was oxidized to sulfoxide, to vary the energy of the CS state. The photophysical properties of the dyads were studied with steady-state and time-resolved UV−vis absorption and luminescence spectroscopy, femtosecond and nanosecond transient absorption spectroscopic methods, time-resolved electron paramagnetic resonance (TREPR) spectroscopy, as well as theoretical computations. We found different photophysical properties for these dyads as compared to previously reported analogous dyads containing flexible linkers between the donor and the acceptor. Notably, long-lived CS states are observed for these compact dyads.

2. EXPERIMENTAL SECTION

2.1. General Method. Compounds **NI-1**, **NI-2**, **NI-3**, **NI-PTZ-1**, **NI-PTZ-2**, **NI-PTZ-3**, **NI-PTZ-O**, and **NI-Ph** were synthesized according to the literature methods.[52−54] All of the chemicals used in the synthesis are analytically pure. The synthesis procedures and the molecular structure characterization data can be found in the Supporting Information. ^{1}H and ^{13}C NMR spectra were recorded on a Bruker 400/500 MHz spectrometer, respectively ($CDCl_3$ or dimethyl sulfoxide (DMSO)-d_6 was used as the solvent, tetramethylsilane (TMS) as the standard for which δ = 0.00 ppm). High-resolution mass spectrometry (HRMS) was determined with a LTQ Orbitrap XL MS spectrometer or matrix-assisted laser desorption ionization time-of-flight mass spectrometry (MALDI-TOF MS). UV−vis absorption spectra of the compounds were measured on a UV2550 spectrophotometer (Shimadzu Ltd., Japan). The fluorescence emission spectra were recorded on a FS5 spectrofluorometer (Edinburgh Instruments, U.K.). The luminescence lifetimes were measured on an OB920 luminescence lifetime spectrometer (Edinburgh Instruments, U.K.).

2.2. Synthesis of NI-PTZ-1. This compound was synthesized following a modified literature method.[54] Under N_2 atmosphere, **NI-1** (50.0 mg, 0.13 mmol) and 10-*H*-phenothiazine (40.0 mg, 1.97 mmol) were dissolved in dry toluene (TOL, 5 mL). After purging with N_2 for 20 min, K_2CO_3 (55.0 mg, 3.95 mmol) was added into the reaction mixture, followed by $Pd(OAc)_2$ (3.0 mg, 0.01 mmol) and $(t\text{-}Bu)_3PHBF_4$ (11.0 mg, 0.04 mmol). The mixture was refluxed at 150 °C for 2 h. After cooling to room temperature, DCM was added to the reaction system and then the mixture was poured into water. The mixture was extracted with DCM (3 × 10 mL). Then, the organic layer was washed with brine (2 × 50 mL) and dried over anhydrous Na_2SO_4. The solvent was removed under reduced pressure. The crude product was dissolved with DCM (1 mL) and *n*-hexane (HEX) (8 mL) was added to precipitate the yellow solid. Then, the product (54.4 mg, yield: 84%) was filtered out. m.p.: >250 °C. ^{1}H NMR ($CDCl_3$, 400 MHz): δ 8.71−8.69 (d, J = 8.0 Hz, 2H), 8.34−8.32 (d, J = 8.0 Hz, 2H), 7.87−7.83 (m, 2H), 7.03−7.01 (d, J = 8.0 Hz, 2H), 6.95−6.91 (m, 2H), 6.85−6.81 (m, 1H), 6.44−6.42 (d, J = 8.0 Hz, 2H), 2.21 (s, 6H). Ion Trap HRMS-ESI$^+$: calcd M^+, m/z = 498.1402; found $[M + H]^+$, m/z = 499.1484; $[M + Na]^+$, m/z = 521.1303.

2.3. Synthesis of NI-PTZ-2. The synthesis procedure is similar to that of **NI-PTZ-1**. Yield: 59%. m.p.: >250 °C. ^{1}H NMR ($CDCl_3$, 400 MHz): δ 8.70−8.68 (d, J = 8.0 Hz, 2H), 8.33−8.31 (d, J = 8.0 Hz, 2H), 7.86−7.83 (m, 2H), 7.44−7.36 (m, 3H), 7.06−7.04 (d, J = 8.0 Hz, 2H), 6.96−6.92 (m, 2H), 6.87−6.83 (m, 2H), 6.46−6.43 (d, J = 12.0 Hz, 2H), 2.24 (s, 3H). ^{13}C NMR ($CDCl_3$, 125 MHz): δ 163.94, 139.18, 134.53, 134.18, 131.87, 131.74, 130.98, 128.74, 127.16, 127.03, 122.71, 116.91, 17.90. Ion Trap HRMS-ESI$^+$: calcd M^+, m/z = 484.1245; found $[M + H]^+$, m/z = 485.1320; $[M + Na]^+$, m/z = 507.1143.

2.4. Synthesis of NI-PTZ-3. The synthesis procedure is similar to that of **NI-PTZ-1**. Yield: 95%. m.p.: >250 °C. ^{1}H NMR ($CDCl_3$, 400 MHz): δ 8.69−8.67 (d, J = 8.0 Hz, 2H), 8.32−8.30 (d, J = 8.0 Hz, 2H), 7.85−7.81 (m, 2H), 7.56−7.51 (m, 4H), 7.08−7.06 (d, J = 8.0 Hz, 2H), 6.96−6.93 (m, 2H), 6.88−6.84 (m, 2H), 6.47−6.45 (d, J = 8.0 Hz, 2H). Ion Trap HRMS-ESI$^+$: calcd M^+, m/z = 470.1089; found $[M + H]^+$, m/z = 471.1156; $[M + Na]^+$, m/z = 493.0982.

2.5. Synthesis of NI-PTZ-O. Compound **NI-PTZ-1** (160 mg, 0.32 mmol) was dissolved in acetic acid (20 mL). The reaction mixture was heated at 50 °C, and then 30% H_2O_2 (20 equiv) was added. After reacting for 2 h, the reaction had completed, and the color of the solution changed from bright yellow to light yellow. After cooling to room temperature, the solvent was removed under reduced pressure. The crude product was further purified with column chromatography (silica gel, DCM/ethyl acetate = 1:1, v/v) to give a cyan solid (31 mg, yield: 19%). m.p.: >250 °C. ^{1}H NMR (DMSO-d_6, 400 MHz): δ 8.65−8.61 (m, 4H), 8.09−8.08 (m, 2H), 8.01−7.99 (m, 2H), 7.68−7.66 (m, 2H), 7.41 (s, 2H), 7.36−7.34 (m, 2H), 6.82−6.81 (d, J = 4.0 Hz, 2H), 2.18 (s, 6H). ^{13}C NMR ($CDCl_3$, 125 MHz): δ 163.46, 139.57, 139.10, 138.76, 135.20, 134.77, 132.81, 131.94, 131.89, 131.81, 129.99, 128.89, 127.24, 122.49, 122.11, 117.74, 18.15. Ion Trap HRMS-ESI$^+$: calcd M^+, m/z = 484.1245; found $[M + H]^+$, m/z = 515.1442; $[M + Na]^+$, m/z = 537.1234.

2.6. Electrochemical Studies. Cyclic voltammetry curves were recorded with a CHI610D electrochemical workstation (CHI instruments, Inc., Shanghai, China). The counter electrode is a platinum electrode; a glassy carbon electrode is the working electrode. The ferrocenium/ferrocene (Fc^+/Fc) redox couple was used as an internal reference. Spectroelectrochemistry was performed using a 0.1 cm path length quartz electrochemical cell. A platinum gauze was the working electrode, and a platinum wire was the counter electrode. The potential was regulated with a CHI610D electrochemical workstation, and the spectra were recorded with an Agilent 8453 UV−vis spectroscopy system (Agilent Technologies Inc.). In both cases, $Bu_4N[PF_6]$ was used as the supporting electrolyte, and the $Ag/AgNO_3$ (0.1 M in acetonitrile (ACN)) couple was used as the reference electrode. Samples were deaerated with N_2 for ca. 15 min before measurement, and the N_2 atmosphere was kept during the measurement.

2.7. Nanosecond Transient Absorption Spectroscopy. Nanosecond transient absorption spectra were measured with a LP920 laser flash photolysis Spectrometer (Edinburgh Instruments, U.K.). The transient signals were digitized on a Tektronix TDS 3012B oscilloscope. All samples were purged with N_2 for

https://doi.org/10.1021/acs.jpcb.3c02595
J. Phys. Chem. B XXXX, XXX, XXX−XXX

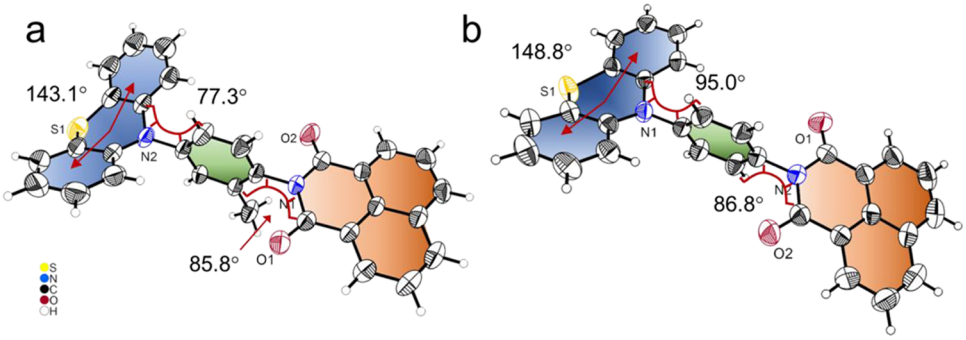

Figure 1. Oak Ridge thermal ellipsoid plot (ORTEP) view of the molecular structures of (a) **NI-PTZ-2** and (b) **NI-PTZ-3** determined by single-crystal X-ray diffraction (50% probability thermal ellipsoids).

15 min before measurements if needed to be measured in a N_2-saturated solution. The data were analyzed with the L900 software.

2.8. Femtosecond Transient Absorption Spectroscopy. Pump−probe experiments were performed on a setup based on a regenerative amplifier Ti:sapphire laser (Legend, Coherent), pumped by a Ti:sapphire oscillator (Micra, Coherent). The system produces 40 fs pulses at 800 nm, at 1 kHz repetition rate with an average 3.2 W power. The pump pulses at 345 nm were obtained by second harmonic generation of the 690 nm signal beam produced by sending a portion of the fundamental laser radiation to a commercial Optical Parametric Amplifier (Topas, Light Conversion).

The probe beam has been obtained by focusing another small portion of the fundamental laser output on a 3-mm-thick calcium fluoride window, generating a white light continuum covering the 375−750 nm spectral window. The white light is then split into a probe and reference beam using a 50% beam splitter. Pump−probe delays are introduced by sending the fraction of the pulse used to generate the white light to a motorized translation stage. Both pump and probe are spectrally overlapped at the sample position, and after crossing into the sample, the probe and reference beams are sent through a spectrograph coupled to a home-made detector. The sample solution was contained in a 2 mm quartz cuvette, mounted on a movable stage to avoid photodegradation and multiple excitations. The data were analyzed by means of singular value decomposition and global analysis, employing the software Glotaran.[55]

2.9. Single-Crystal X-ray Diffraction. The single crystals of **NI-PTZ-2** and **NI-PTZ-3** were obtained by slow diffusion of HEX into DCM solution of the compounds. The X-ray diffraction data of the single crystals were measured and collected on a Bruker SMART APEX CCD diffractometer with graphite-monochromatized Mo Kα radiation (λ = 0.71073 Å) at 298 K, using the SMART and SAINT programs. The X-ray diffraction data were treated with the program SHELXTL-2018 applying contained space-group determination (XPREP), direct method structure solution (XS), and least-squares refinement (XL).[56−58] CCDC 2079275 (**NI-PTZ-2**) and 2079274 (**NI-PTZ-3**) contain the supporting crystallographic data for this paper and the data can be obtained freely from the Cambridge Crystallographic Data Centre via https://www.ccdc.cam.ac.uk/.

2.10. Time-Resolved Electron Paramagnetic Resonance (TREPR) Spectra. Samples were dissolved in frozen solution TOL/(2-methyltetrahydrofuran, 2-MeTHF) (1/1, v/v) with a concentration of 1×10^{-4} M and transferred into 4.5 mm OD, 3.0 mm ID quartz tubes. The measurements of time-resolved continuous-wave (CW) EPR were performed on an X-band EPR Elexsys E-580 spectrometer (Bruker) with the dielectric ring X-Band ER 4118X-MD5-W1 resonator at a temperature of 80 K. The oxygen was removed with five freeze−pump−thaw cycles. Optical excitation was carried out by an Nd:YAG pulse laser (LQ629 Solar LS) at a wavelength of 355 nm with a pulse energy of 1 mJ and frequency of 100 Hz. The spectra were simulated using the EasySpin package based on Matlab.[59]

3. RESULTS AND DISCUSSION

3.1. Molecular Structure Designing Rationales. NI is a chromophore with high T_1 state energy (2.3 eV),[60] and electron accepting ability (reduction potential, E_{RED} = −1.82 V, vs Fc/Fc$^+$). PTZ is a well-known electron donor (oxidation potential, E_{OX} = +0.3 V, vs Fc/Fc$^+$).[61] The previously studied NI-PTZ dyads containing a flexible linker show CS states formation upon photoexcitation, whose spin multiplicity was not determined, with a lifetime of ca. 300 ns.[60] In order to form ^{3}CS states, compact dyads are desired.[62] Recently, we studied the CT in a NI-PTZ compact dyad, with the NI and PTZ moieties connected with a C−N single bond, observing a long-lived CS state (2.6 μs).[63] In this work, we connect the NI and PTZ moieties via a 1,4-phenylene linker at the amide N-position of NI and the N-position of the PTZ moiety (Scheme 1). One or two methyl groups are introduced on the phenylene linker to exert conformational restriction (**NI-PTZ-1**, **NI-PTZ-2**, and **NI-PTZ-3**) and tune the electronic coupling magnitude, while keeping the ^{1}LE and CS states energy constant. We furthermore analyzed a compound with an oxidized PTZ moiety (**NI-PTZ-O**). The CS-state energy of the oxidized compound will increase, while the ^{3}NI* state and the coupling between the two states will be kept constant to a large extent, inducing a perfect comparison for the photochemistry studies.

The synthesis of the dyads is based on the routine derivatization chemistry of NI and PTZ chromophores (Scheme 1). The molecular structures were fully verified with ^{1}H NMR, ^{13}C NMR, and HRMS analysis. **NI-PTZ-1** was reported previously, the TADF properties in solid state were studied, but the CT mechanism was not studied in detail.[54] The steady-state UV−vis absorption and femtosecond transient absorption spectra of **NI-PTZ-3** were reported recently,[52] but the TADF properties and the long-lived CS state were not studied.

The molecular structures of **NI-PTZ-2** and **NI-PTZ-3** were determined by single-crystal X-ray diffraction (Figures 1 and S15). The crystallographic data are compiled in Table S1. Each unit cell of **NI-PTZ-2** contains four molecules and has a

https://doi.org/10.1021/acs.jpcb.3c02595
J. Phys. Chem. B XXXX, XXX, XXX−XXX

monoclinic crystal structure. Four molecules of **NI-PTZ-3** stack to form a triclinic cell. We observed weak $\pi-\pi$ intermolecular interactions between the adjacent NI moieties in the single crystals of **NI-PTZ-2**, and the distance between the parallel planes of NI is 3.437 Å. In **NI-PTZ-3**, there is no $\pi-\pi$ intermolecular interaction between the adjacent NI moieties, and the dihedral angle between the adjacent NI planes in the single crystals is 85.4° (Figure S15c). For **NI-PTZ-1**, growing a single crystal with satisfactory quality for X-ray diffraction study failed.

The torsion angles between the PTZ moiety and the linker (benzene) are 77.3 and 95.0° for **NI-PTZ-2** and **NI-PTZ-3**, respectively (Figure 1). The dihedral angle of the π-conjugation planes of the NI moiety and the linker in **NI-PTZ-2** is 85.8°, which is similar to that in **NI-PTZ-3** (86.8°). The PTZ moieties adopt the well-known slightly puckered geometry, with dihedral angles between the two phenyl rings in the PTZ units as 36.9° (or 143.1°) and 31.2° (or 148.8°) for **NI-PTZ-2** and **NI-PTZ-3**, respectively. Furthermore, the dihedral angles between the planes of NI and PTZ are 14.6° in **NI-PTZ-2** and 23.1° in **NI-PTZ-3**. The centroid (NI)−centroid (PTZ) distance is 9.822 Å for **NI-PTZ-2**, and a similar result is observed in **NI-PTZ-3** (9.818 Å). These distances are much shorter compared to the previously reported NI-PTZ dyads with flexible linkers, which are in the range of 14.5−17.5 Å (in the extended conformation, not the folded, or the coiled conformation).[60]

The ground-state (S_0) geometries of **NI-PTZ-1**, **NI-PTZ-2**, and **NI-PTZ-3** were optimized at the B3LYP/6-31G(d) level (Figure S16). According to density functional theory (DFT) optimization, the dihedral angles between the NI moiety and the phenyl linker for the three dyads are similar (−90.1, −89.7, and −90.2°, respectively). The planes of the NI and PTZ moieties form dihedral angles of 16.3° in **NI-PTZ-1**; similar results are observed for the other two dyads (13.9° for **NI-PTZ-2** and 16.5° for **NI-PTZ-3**). The dihedral angles between the two phenyl rings of the PTZ moiety are 29.9, 30.2, and 30.2° for **NI-PTZ-1**, **NI-PTZ-2**, and **NI-PTZ-3**, respectively. The centroid (NI)−centroid (PTZ) distances are both 9.859 Å for **NI-PTZ-1** and **NI-PTZ-2**, and a similar result is observed in **NI-PTZ-3** (9.867 Å). For all dyads, the difference between experimental and calculated structures is not significant.

3.2. Steady-State UV−Vis Absorption and Luminescence Spectra. UV−vis absorption spectra of the dyads were studied (Figure 2). For all systems, a broad absorption band in the range of 275−350 nm was observed, which is assigned to the NI moiety by comparison with the absorption spectrum of the reference compound **NI-Ph**. Moreover, a sharp absorption band was observed at 256 nm, which is attributed to the PTZ moiety.[61] The absorption profile of the compounds in the range of 275−350 nm indicates that the electronic coupling between the NI and PTZ moieties is negligible at the ground state. The extremely weak absorption bands in the 350−375 nm region of the spectrum of **NI-PTZ-1−3** are attributed to the absorption from the ground state to the CT state ($S_0 \rightarrow {}^1$CT transition), due to the very weak, even negligible electronic coupling between the NI and the PTZ moieties at the ground state. This result is similar to that of the previously reported NI-PTZ dyads containing long, flexible polymethylene linkers,[60,64] However, it is different from the previously reported NI-PTZ compact dyad, containing a direct C−N connection between the two moieties,[63] for which a weak, broad absorption band (due to $S_0 \rightarrow {}^1$CT transition) was observed in the 375−525 nm range.[63] The weak coupling in the current dyads is in line with our molecular structure design rationales. It should be pointed out that negligible coupling in the current dyads at the ground state does not necessarily exclude observable coupling at the excited state. From the LE absorption band (^{1}NI*) and CT emission band (Figures 2 and 3), the coupling matrix elements (V_{DA}) between $D^{+\bullet}-A^{-\bullet}$ (FC) and DA (S_0) can be obtained by using eqs S1 and S2.[63,65] For **NI-PTZ-1**, the value of V_{DA} is 0.10 eV. Reducing the number of methyl groups on the linker strengthens the coupling between the CS state and the LE state, which are 0.30 eV for **NI-PTZ-2** and 0.31 eV for **NI-PTZ-3**, respectively (Table S8). For the oxidized compound **NI-PTZ-O**, the V_{DA} between the LE state and the CS state is smaller (0.12 eV).

The steady-state fluorescence spectra of the dyads were measured (Figure 3). A broad, structureless emission band centered at 620 nm was observed for the dyads, but not for the reference compound **NI-Ph** (Figure 3a). It is unlikely that this fluorescence is due to the PTZ moiety because it emits at wavelengths <500 nm.[66] The NI moiety has an emission band centered at 378 nm.[67] A similar emission band was observed for the previously reported NI-PTZ dyads containing flexible linkers, and it was attributed to the intramolecular exciplex emission. Exciplexes can form in coiled conformations for the previously reported flexible dyad where the NI and PTZ moieties have face-to-face interaction.[64] In the current compact dyads containing a rigid 1,4-phenylene linker, however, such a bent geometry is excluded; thus, we attribute the broad emission band centered at 620 nm to a CT-state emission, as already observed for the compact NI-PTZ dyad containing the C−N linker.[63] These results indicate that the ^{1}CT/S_0 coupling is nonnegligible for these dyads, although no significant coupling was observed from the UV−vis absorption spectra. Interestingly, we found that among the three dyads, more conformational restriction leads to a weaker CT emission, i.e., **NI-PTZ-1** gives the weakest emission, whereas **NI-PTZ-3** gives the strongest emission among the three dyads. This trend is confirmed by luminescence quantum yield measurements (Table 1).

We furthermore observed that the CT emission band is highly sensitive to oxygen (O_2, Figure 3b). For instance, the emission intensity of **NI-PTZ-1** is intensified by 55-fold in deaerated CHX solution as compared to that of the aerated solution. This is an indication of the possible involvement of the triplet state in the emission processes because the ordinary emissive S_1 state (or fluorescence) is usually much less sensitive to O_2. The emission cannot simply be assigned to phosphorescence, based on the oxygen sensitivity, since normally structured emission bands should be observed for the phosphorescence of organic chromophores, due to the vibronic coupling-enhanced $T_1 \rightarrow$

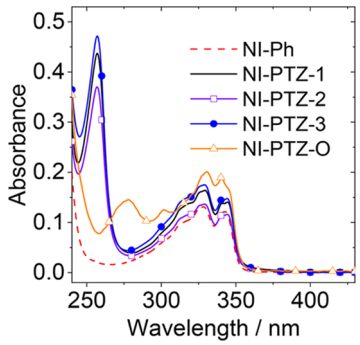

Figure 2. UV−vis absorption spectra of the compounds in cyclohexane (CHX), $c = 1.0 \times 10^{-5}$ M, 20 °C.

https://doi.org/10.1021/acs.jpcb.3c02595
J. Phys. Chem. B XXXX, XXX, XXX−XXX

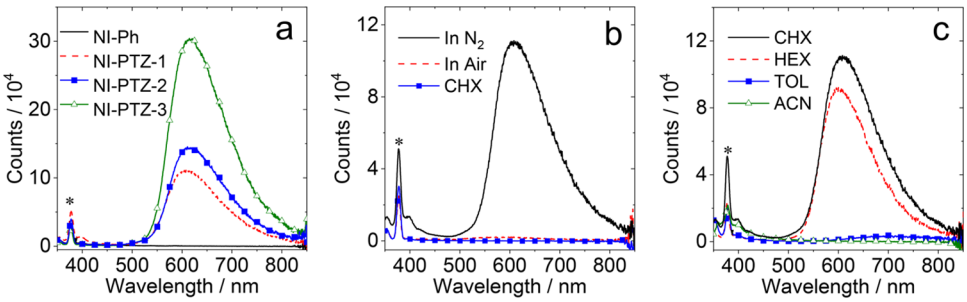

Figure 3. (a) Fluorescence emission spectra of **NI-Ph**, **NI-PTZ-1**, **NI-PTZ-2**, and **NI-PTZ-3** in CHX under nitrogen atmosphere; fluorescence emission spectra of **NI-PTZ-1** (b) in CHX under different atmospheres (N_2, air) and (c) in different solvents under N_2. λ_{ex} = 340 nm, $c = 1.0 \times 10^{-5}$ M, 20 °C. The asterisks indicate the Raman scattering peak.

Table 1. Photophysical Parameters of Compounds

	λ_{abs} [a]	ε [b]	λ_F [c]	Φ_Δ [d]	τ_T [e]	Φ_F [f]	τ_F [g]	τ_F [h]	τ_P [i]
NI-Ph	328/343	1.3/1.2	–[i]	2	153.7	0.4	–[j]	–[j]	455.0
NI-PTZ-O	331/340	2.0/1.9	601[k]	35	191.1	0.5[k]	–[j]	10.0[k]	464.8
NI-PTZ-1	329/345	1.6/1.4	612	30	274.7[l]	1.1	13.8 ns/321.6 μs	14.4	426.4
NI-PTZ-2	329/344	1.4/1.2	611	36	193.4[l]	2.2	11.1 ns/280.4 μs	13.9	383.7
NI-PTZ-3	329/344	1.8/1.5	615	38	180.3[l]	2.7	10.3 ns/142.6 μs	13.2	410.6

[a]Maximal UV−vis absorption wavelength (1.0×10^{-5} M) in CHX, in nm. [b]Molar absorption coefficient, in 10^4 M^{-1} cm^{-1}. [c]Maximal fluorescence emission wavelength in CHX, in nm. [d]Singlet oxygen ($^1O_2$) quantum yield (Φ_Δ) (λ_{ex} = 320 nm) with $Ru(bpy)_3[PF_6]_2$ as standard (Φ_Δ = 57% in DCM) in CHX, in %. [e]Triplet excited-state lifetimes, in deaerated CHX, in μs. [f]Fluorescence quantum yields under N_2 atmosphere, in %. [g]Fluorescence lifetimes under N_2. [h]Fluorescence lifetimes under air atmosphere, in ns. [i]Phosphorescence lifetimes at 540 nm in 77 K, in ms. [j]Not applicable. [k]In DCM. [l]Intrinsic triplet-state lifetimes. Obtained by fitting the experimental curves based on the kinetic model with the TTA self-quenching effect considered, in μs.

S_0 radiative decay process.[68] This atmosphere-dependent fluorescence emission was not reported for the NI-PTZ dyad containing flexible linkers.[64] We observed similar luminescence features for the compact NI-PTZ dyads containing a single-bond C−N linker, which was attributed to TADF.[63] The CS-state energy of **NI-PTZ-1** can be approximated by the onset of the CT emission band, as ca. 2.48 eV. This energy is literally the same as the ^{3}NI* state energy (2.30 eV).[60,69] Thus, TADF is a plausible mechanism to explain the O_2-sensitive luminescence of the dyads. The CT band centered at 610 nm can be observed in CHX for all of the three dyads, suggesting the occurrence of TADF in this solvent. The CT emission band is also sensitive to the solvent polarity (Figure 3c). A weak emission band centered at 710 nm in deaerated TOL was observed for **NI-PTZ-1**, but not for the other two dyads (Figures 3c and S18). In acetonitrile (ACN), no emission was observed for all of the three dyads. This result can be explained by the decreased CS-state energy in polar solvents and the energy gap law, whereas the ^{3}LE state energy is less sensitive to solvent polarity.[60] For **NI-PTZ-O**, a weak emission band centered at 600 nm was observed (Figure S19), which is not sensitive to O_2, suggesting that the triplet state is not involved in the emission process of this dyad.

We furthermore determined the luminescence lifetimes under different atmospheres for all compounds (Figures 4, S22, and S23). Under N_2 atmosphere, the luminescence decay trace of **NI-PTZ-1** shows drastically different phases (Figure 4a). The early phase, recorded using a pulsed EPL picosecond laser (the IRF of the luminescence spectrometer is 0.1 ns), is characterized by a fast decay (lifetime τ = 13.8 ns, population ratio: 42%), followed by a slow-decaying component (τ = 321.6 μs, population ratio: 58%, at a concentration of 10 μM, excited with a microsecond flash xenon lamp). The rate constants of ISC (k_{ISC}), rISC (k_{rISC}), and triplet-state nonradiative decay (k_{nr}^T) of **NI-PTZ-1** in CHX were estimated to be 7.2×10^7, 1.4×10^4, and 3.1×10^3 s^{-1}, respectively (eqs S3−S5, referring to the Supporting Information for details). Similar results were observed for **NI-PTZ-2** (11.1 ns (41%)/280.4 μs (59%), at 12 μM, Figure S22) and **NI-PTZ-3** (10.3 ns (64%)/142.6 μs (36%) at 15 μM, Figure S23). Note that among the three dyads, we found a clear trend that a more significant molecular conformational restriction leads to longer emission lifetime. We also found that the luminescence lifetime of the compounds is only slightly varied at different concentrations (**NI-PTZ-1**, 377.8 μs at 6 μM; 396.0 μs at 4 μM, Figure S21). Thus, we attribute the long-lived luminescence to TADF, rather than to P-type delayed fluorescence due to a TTA effect (which is an intermolecular diffusion-controlled process).[70] The previously reported NI-PTZ dyads that have a long, flexible polymethylene linker show a CT emission lifetime of ca. 5 ns, and no long-lived component in the fluorescence decay trace was reported.[60,64]

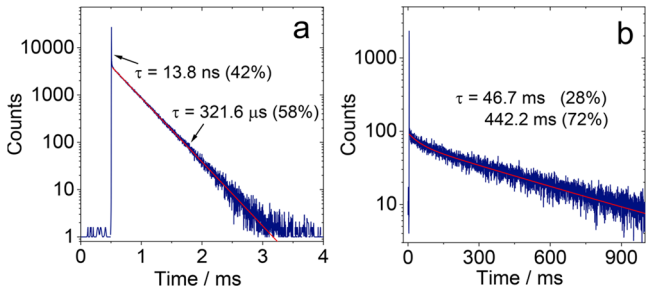

Figure 4. Fluorescence lifetime decay traces of **NI-PTZ-1**: (a) monitored at 600 nm (13.8 ns was measured with EPL picosecond laser), and another component of 321.6 μs was monitored with microsecond flash xenon lamp, c = ca. 1.0×10^{-5} M, in deaerated CHX, at 298 K; (b) at 540 nm, $c = 1.0 \times 10^{-4}$ M, in deaerated EtOH/MeOH (4:1, v/v), at 77 K, excited with microsecond flash xenon lamp, λ_{ex} = 340 nm.

https://doi.org/10.1021/acs.jpcb.3c02595
J. Phys. Chem. B XXXX, XXX, XXX−XXX

The delayed fluorescence of the current dyads has a much longer lifetime than that observed for the compact NI-PTZ dyad with a C−N bond linker (22.6 ns (96.6%)/2.6 μs(3.4%)).[63] These differences can be attributed to the delicate energy-level ordering of ^{3}CT and ^{3}LE states.[63] In the current dyads, the CS-state energy is slightly higher than the ^{3}LE state, and the energy pooling effect of the ^{3}LE state makes the delayed fluorescence lifetime longer than the previously reported compact NI-PTZ dyad, for which the CS state is lightly lower in energy than the ^{3}LE state.[63] This is supported by nanosecond transient absorption studies (vide infra). In solvents that are more polar than CHX, such as TOL and ACN, no TADF was observed (the luminescence is extremely weak).

The observation of long-lived components in the luminescence decay trace strongly suggests the involvement of triplet states in the radiative decay of the singlet excited state, which is typical for TADF.[38,71−74] In order to further confirm this postulate, the luminescence lifetimes of the dyads in aerated solution were also studied. The luminescence lifetime of **NI-PTZ-1** was shortened to 2.0 ns (47%)/15.8 ns (53%) in aerated solution (Figure S24). The prompt luminescence lifetime of 13.8 ns was not quenched and maintained as 15.8 ns (the difference is probably due to determination uncertainty). The 2.0 ns component is probably due to the nonradiative transition process of the ^{1}CS state, e.g., ISC to ^{3}NI*. The quenched delayed lifetime was not observed (with the lifetime of 321.6 μs in deaerated CHX) as a result of the slow rISC rate and substantially quenched ^{3}NI* triplet state in aerated CHX. Similar results were obtained for **NI-PTZ-2** and **NI-PTZ-3** (Figure S24). The lifetime of the CT emission centered at 600 nm of **NI-PTZ-O** is 10.0 ns in aerated solution (Figure S27), which is shorter than the others.

These results correlate to the electronic coupling and the relative energy order of the CT/^{3}LE states. For NI-PTZ dyads containing a long, flexible polymethylene linker (polymethylene), it was supposed that the bent conformation leads to face-to-face intramolecular interaction between the NI and PTZ moieties, determining a much shorter CT emission lifetime (ca. 5 ns).[64] The single exponential decay of the luminescence excludes any possibility of involvement of triplet states in the emission process. Moreover, considering the fast conformational fluctuations in solution, establishing of an equilibrium between the CS state and the ^{3}NI* state is unlikely. In the current compact dyads, the electronic coupling should be much weaker than that established with the face-to-face interaction, which increases the prompt fluorescence lifetime (10.3−13.8 ns) and opens up the possibility of TADF. This postulation is supported by the observation of an increased prompt fluorescence lifetime for the recently reported compact NI-PTZ dyad presenting a short C−N linker (22.6 ns).

The excimer emission quantum yields (~0.004) and the luminescence lifetimes (1.28−5.35 ns) of the previously studied flexible NI-PTZ dyad are lower or shorter than the current compact dyads. **NI-PTZ-1−3** show CS-state emission quantum yields of 0.011−0.027 and prompt fluorescence lifetimes of 10.3−13.8 ns. Also, a slow rise phase (60−1300 ps) was observed for the previous exciplex emission,[64] but it is not observed for the current compact dyads (Figure 4a, the IRF of the luminescence lifetime spectrometer is ca. 100 ps).

NI-PTZ-1 has the longest prompt fluorescence lifetime (13.8 ns), and this dyad has the smaller electronic coupling (V_{DA} 0.10 eV), whereas **NI-PTZ-3**, with the strongest electronic coupling between the donor and the acceptor (0.31 eV), has the shortest prompt fluorescence lifetime (10.3 ns). These results indicate that the geometry, rigidity of the linker and electronic coupling between the units play an important role in determining the photophysical properties of donor−acceptor dyads.

In order to determine the ^{3}NI* state energy of the dyads, we measured their phosphorescence emission spectra in frozen solution (EtOH/MeOH, 4:1, v/v) at 77 K (Figure S25). For **NI-Ph**, two structured emission bands in the ranges of 350−450 and 500−650 nm were observed. The emission band in the shorter wavelength range is assigned to fluorescence and the emission band at lower energy is attributed to phosphorescence.[69] This is supported by the luminescence lifetime studies since the emission band in the short wavelength range has a lifetime of 0.15 ns (92%)/1.39 ns (8%), whereas the second emission band has a lifetime of 455 ms (Figure S25). From the onset of the phosphorescence band at the high energy side (can be approximated as the vibrational 00 transition of $T_1 \rightarrow S_0$ radiative relaxation), the ^{3}NI* state energy is approximated as 2.30 eV.

For all of the dyads, phosphorescence bands similar to that of **NI-Ph** were observed (Figure S25). The phosphorescence of the dyads shows a biexponential decay. For instance, **NI-PTZ-1** shows a phosphorescence lifetime of 46.7 ms (28%)/442.2 ms (72%) (Figure 4b). The major components of the phosphorescence lifetime of **NI-PTZ-2** and **NI-PTZ-3** are 458.0 and 432.4 ms, respectively (Figure S25). No CT emission band was observed, which is likely due to the increased CS-state energy in the frozen solution.

3.3. Electrochemistry Study. The redox potentials of the dyads were measured with cyclic voltammetry (Figure 5). For

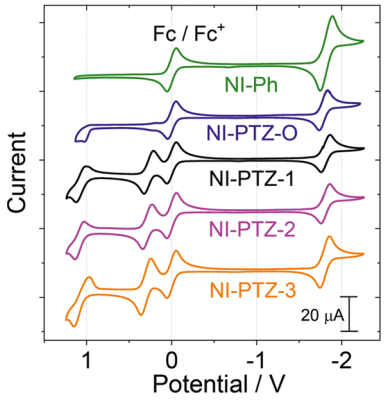

Figure 5. Cyclic voltammogram of compounds. Ferrocene (Fc) was used as an internal reference (set as 0 V in the cyclic voltammograms), in deaerated DCM containing 0.10 M $Bu_4N[PF_6]$ as the supporting electrolyte. Scan rates: 50 mV s^{-1}, $c = 1.0 \times 10^{-3}$ M, 20 °C.

NI-Ph, a reversible reduction wave was observed at −1.82 V (vs Fc/Fc^+), while no oxidation wave was observed in the potential window used in the experiment. For **NI-PTZ-1**, a similar reduction wave was observed (Figure 5). Moreover, two reversible oxidation waves at +0.28 and +1.07 V (vs Fc/Fc^+) were observed, which are attributed to the PTZ moiety.[61] Similar results were observed for the other dyads (Figure 5). The similarity of the redox potentials of the isolated PTZ and NI moieties and those measured for the dyads indicates negligible interactions between the donor and the acceptor at the ground state. These results also indicate that PTZ is the electron donor and NI is the electron acceptor for the dyads upon photoexcitation, although NI can act as an electron donor in the

https://doi.org/10.1021/acs.jpcb.3c02595
J. Phys. Chem. B XXXX, XXX, XXX−XXX

Table 2. Redox Potentials (E_{OX} and E_{RED}), Driving Forces of Charge Separation (ΔG_{CS}), and the Energy of the CSS of Compounds (E_{CS}) in Different Solvents[a]

			ΔG_{CS} (eV)					E_{CS} (eV)				
	E_{OX}[b] (V)	E_{RED}[b] (V)	HEX	CHX	TOL	DCM	ACN	HEX	CHX	TOL	DCM	ACN
NI-Ph	–[c]	−1.82	–[c]	–[c]	–[c]	–[c]	–[c]	–[c]	–[c]	–[c]	–[c]	–[c]
NI-PTZ-O	+1.02	−1.78	−0.16	−0.22	−0.32	−0.89	−1.13	3.36	3.30	3.20	2.63	2.39
NI-PTZ-1	+0.28/+1.07	−1.81	−0.87	−0.93	−1.03	−1.61	−1.92	2.65	2.59	2.49	1.91	1.60
NI-PTZ-2	+0.29/+1.09	−1.80	−0.87	−0.93	−1.03	−1.61	−1.92	2.65	2.59	2.49	1.91	1.60
NI-PTZ-3	+0.30/+1.06	−1.80	−0.86	−0.92	−1.02	−1.60	−1.91	2.66	2.60	2.50	1.94	1.61

[a]Cyclic voltammetry in N_2-saturated DCM containing a 0.10 M Bu_4NPF_6 supporting electrolyte; Pt electrode was used as the counter electrode; the working electrode is the glassy carbon electrode; $Ag/AgNO_3$ couple is the reference electrode. E_{00} = 3.52 eV. E_{00} is the energy level of the singlet excited state localized on the NI moiety (^{1}NI*) approximated with the crossing point of UV−vis absorption and fluorescence emission spectra after normalization. [b]The value was obtained by setting the oxidation potential of Fc^+/Fc as 0. [c]Not observed or not applicable.

presence of a strong electron acceptor.[75] For **NI-PTZ-O**, a similar reversible reduction wave was observed at −1.78 V (vs Fc/Fc^+), whereas the oxidation wave at +1.02 is irreversible.

Based on the electrochemical data, the driving force of the possible photoinduced CS, i.e., ΔG^0_{CS}, was calculated with the Rehm−Weller equation (eqs 2−5, referring to the Supporting Information for details)

$$\Delta G^0_{CS} = e[E_{OX} - E_{RED}] - E_{00} + G_S \quad (2)$$

$$\Delta G_S = -\frac{e^2}{4\pi\varepsilon_S\varepsilon_0 R_{CC}} - \frac{e^2}{8\pi\varepsilon_0}\left(\frac{1}{R_D} + \frac{1}{R_A}\right)\left(\frac{1}{\varepsilon_{REF}} + \frac{1}{\varepsilon_S}\right) \quad (3)$$

$$\Delta G^0_{CR} = -(\Delta G^0_{CS} + E_{00}) \quad (4)$$

$$E_{CSS} = e[E_{OX} - E_{RED}] + \Delta G_S \quad (5)$$

The results (Table 2) show that the CS from ^{1}NI* is thermodynamically allowed for all of the dyads. The driving force for the CS of **NI-PTZ-O** is smaller than that of the dyads without oxidation due to the poor electron-donating ability of PTZ upon oxidation. The results show that for all dyads, the CS-state energy in CHX is higher than that of ^{3}NI* (2.3 eV), which means the low-lying triplet state is the ^{3}NI* state, which is supported by the nanosecond transient absorption (ns-TA) spectral studies (see later section). In polar solvent ACN, for **NI-PTZ-1**, **NI-PTZ-2**, and **NI-PTZ-3**, the CS-state energy is lower than ^{3}NI*. Thus, for these dyads, the low-lying triplet state may probably be the CS state in ACN. These postulations were confirmed by ns-TA spectral studies (see later section).

We furthermore measured the spectroelectrochemistry of the dyads in order to characterize the absorption bands of the radical anion and cation (Figures 6 and S62−S64). With a negative potential applied (−1.65 V, vs $Ag/AgNO_3$), new absorption bands centered at 417, 490, and 831 nm appeared (Figure 6a), which are attributed to the electrochemically generated radical anion $NI^{-\bullet}$ (Figure 6a). Conversely, with a positive potential applied (+0.58 V, vs $Ag/AgNO_3$), new absorption bands centered at 512 nm and in the range of 700−900 nm were observed, which are attributed to the electrochemically generated radical cation $PTZ^{+\bullet}$ (Figure 6b).[60,76] Similar results were observed for the absorption of $PTZ^{+\bullet}$ by using a chemical oxidation method (Figure S61). With the addition of nitrosonium hexafluorophosphate ($NO[PF_6]$), $PTZ^{+\bullet}$ shows an absorption band centered at 515 nm, and a broad, weak absorption band in the range of 600−850 nm. The absorbance and the concentration of the dyad used in the measurement indicate that the oxidation is quantitative (molar absorption coefficient of $PTZ^{+\bullet}$ at 515 nm: 7000 M^{-1} cm^{-1}). It should be pointed out that the absorption features of the radical anions and radical cations in the photoexcitation-generated CS state for the dyads may be different from the UV−vis absorption spectra of the radical anion or cation, generated by the electrochemical method (Figure 6) because there is an electronic interaction between the anion and the cation for the photogenerated CS state.

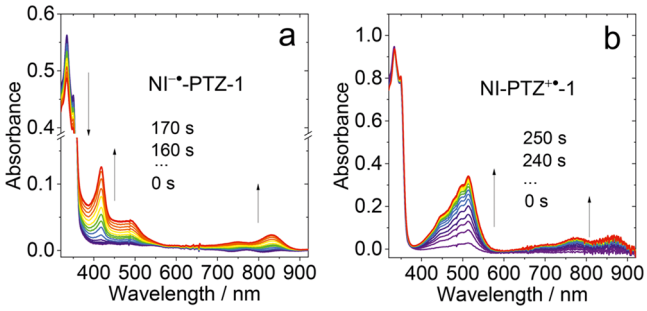

Figure 6. Spectroelectrochemical studies of **NI-PTZ-1**: evolution of the UV−vis absorption spectra with reduction and oxidation potentials applied: (a) upon reduction under −1.65 V, $c = 3.0 \times 10^{-5}$ M and (b) upon oxidation under 0.58 V, $c = 5.0 \times 10^{-5}$ M. The $Ag/AgNO_3$ reference electrode was used. The spectra were recorded in situ with a spectroelectrochemical cell (1 mm optical path), in deaerated DCM, 20 °C.

3.4. Femtosecond Transient Absorption Spectra. The kinetics of photoinduced CS and CR in the three dyads have been studied by ultrafast transient absorption measurements with sub-picosecond time resolution (Figure 7). Three solvents of different polarity (CHX, TOL, and ACN) were used to understand the influence of the microenvironment on the excited-state dynamics of the compounds. All of the spectra have been measured by exciting the samples at 345 nm and the data have been subject to global analysis in order to determine the kinetic constants describing the excited-state dynamics of the dyads. Figure 7a reports the evolution-associated difference spectra (EADS) obtained by globally analyzing the data recorded for **NI-PTZ-1** in TOL, employing a linear decay kinetic scheme with three times constants.

For **NI-PTZ-1**, the initial spectral component (black line in Figure 7a) shows two excited-state absorption (ESA) bands peaked at ca. 400 and 480 nm in CHX. The comparison with the time-resolved spectra recorded for the reference compound **NI-Ph** (see Figure S59) allows to assign this spectral component to the singlet excited state of the NI moiety, which mostly absorbs at 345 nm at ground state. The transient spectra rapidly evolve in

https://doi.org/10.1021/acs.jpcb.3c02595
J. Phys. Chem. B XXXX, XXX, XXX−XXX

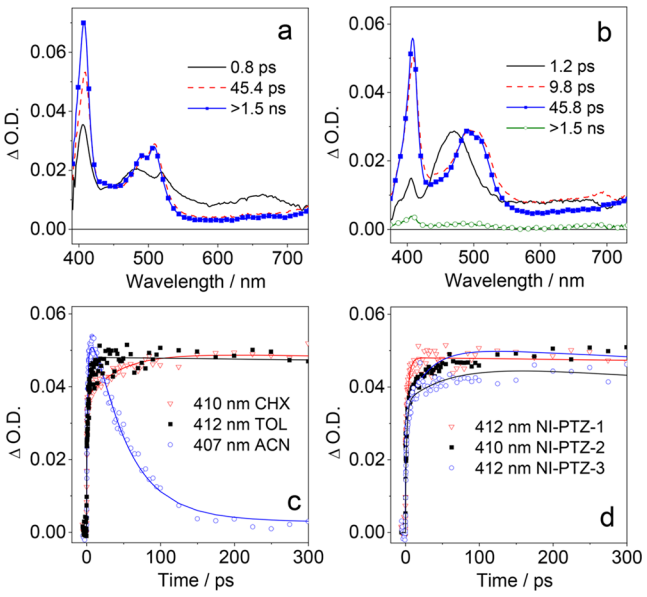

Figure 7. EADS obtained from global analysis of the fs-TA transient absorption data recorded for **NI-PTZ-1** in (a) CHX and (b) ACN. (c) Comparison between the kinetic traces recorded on the maximum of the $NI^{-\bullet}$ absorption band for **NI-PTZ-1** in CHX, TOL, and ACN. (d) Comparison between the kinetic traces recorded on the maximum of the $NI^{-\bullet}$ absorption band in TOL for **NI-PTZ-1**, **NI-PTZ-2**, and **NI-PTZ-3**, λ_{ex} = 345 nm, $c = 1.0 \times 10^{-4}$ M, 20 °C.

about 0.8 ps: within this timeframe, both ESA bands increase in intensity and red shifts, respectively, to 415 and 500 nm. We tentatively assign the evolution observed on the fast 0.8 ps timescale to the occurrence of incomplete CT from the NI toward the PTZ moiety. On the following 45.4 ps, a sharp band peaked at 410 nm develops. Comparison with spectroelectrochemistry results allows to assign this band to $NI^{-\bullet}$, and at the same time, the band peaked at 490 nm to $PTZ^{+\bullet}$. The appearance of those bands confirms the CS. The CS state does not decay by CR within the timescale of the experiment (1.5 ns). When measurements are repeated in the more polar solvent ACN, the kinetics of CS appears to be faster, as inferred by inspecting the EADS presented in Figure 7b. In this case, the sharp band signaling the formation of $NI^{-\bullet}$ is already visible in the second spectral component, rising within 1.2 ps. The following evolution, occurring in 9.8 ps can be interpreted as the vibrational relaxation of the CS state, in which the ESA band shows a time-dependent slight blue shift indicating a typical characteristic of the vibrational cooling. CR appears to be faster in this polar medium: the transient signal indeed mostly recovers within 45.8 ps. The small residual signal shows the typical ESA of the anion and cation species. The transient spectra in TOL are similar to those recorded in CHX, although the dynamics of CS is a bit faster, as noticed by comparing the kinetic traces recorded on the maximum of the $NI^{-\bullet}$ band in the three solvents (see Figure 7c).

The transient spectra measured for **NI-PTZ-2** and **NI-PTZ-3** are very similar to those of **NI-PTZ-1** (Figures S57 and S58), but some variation of the kinetic constants for CS and CR are noticed, see for instance the comparison of the kinetic traces signaling the rise of $NI^{-\bullet}$ in TOL for the three compounds reported in Figure 7d. Additional time-resolved data can be found in the Supporting Information. It should be noted that formation of the ^{3}NI* state cannot be excluded because it is known that the ISC of NI chromophore takes only 10−20 ps.[77] Moreover, the ns-TA spectral analysis shows the formation of the CS state with ^{3}NI* precursor (Figure S31).

Marcus equation (eq 1) was used to study the $-\Delta G^0_{ET}$ dependence on the electron transfer rates in different solvents (CHX, TOL, and ACN, Figure S60).[78,79] The ΔG^0_{ET} of CS and CR are obtained from electrochemical data ($\Delta G_{CR} = -E_{CS}$). The electron transfer rate is determined by fs-TA spectral data, ns-TA spectral data, and fluorescence lifetimes. Based on the fitting results, similar λ values for **NI-PTZ-1**, **NI-PTZ-2**, and **NI-PTZ-3** are estimated as 1.42, 1.47, and 1.48 eV, respectively,

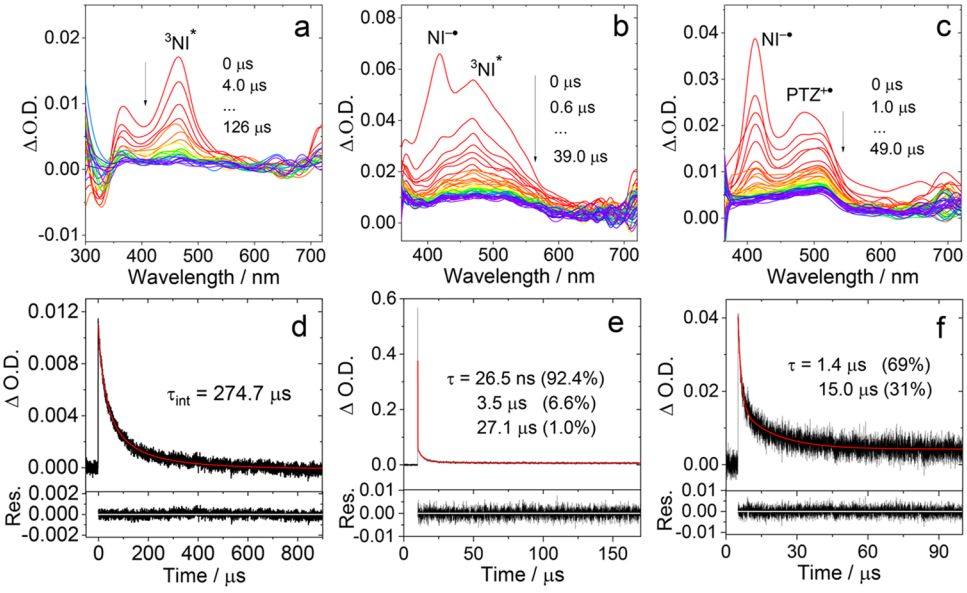

Figure 8. Nanosecond transient absorption spectra of **NI-PTZ-1** in different deaerated solvents of (a) CHX ($c = 1.0 \times 10^{-5}$ M), (b) TOL ($c = 1.0 \times 10^{-4}$ M), and (c) ACN ($c = 2.0 \times 10^{-4}$ M). The corresponding decay traces are at (d) 470 nm, (e) 420 nm, and (f) 420 nm. The intrinsic triplet-state lifetime (τ_{int}) is obtained by fitting the experimental decay traces based on the kinetic model with the TTA self-quenching effect considered in panel (d), λ_{ex} = 355 nm, 20 °C.

https://doi.org/10.1021/acs.jpcb.3c02595
J. Phys. Chem. B XXXX, XXX, XXX−XXX

while V values are estimated as 31.8, 21.9, and 20.2 cm^{-1}, respectively. For these dyads, the CS process in different solvents is located in the Marcus normal region, whereas the CR is in the Marcus inverted region.

Marcus equation can be transformed into the linear expression shown in eq S10. There is linear correlation between $[k_BT \ln k_{ET} + (\Delta G^0_{ET}/2)]$ and $(\Delta G^0_{ET})^2$ for these dyads as shown in Figure S60. The estimated λ and V values for **NI-PTZ-1** are determined as 1.42 eV and 37.9 cm^{-1}. For the same compound, the estimated λ and V values are similar based on different methods.

3.5. Nanosecond Transient Absorption Spectra: Detection of ^{3}NI* and CS States. In order to evaluate the excited-state dynamics of the dyads, we measured their nanosecond transient absorption (ns-TA) spectra (Figures 8 and S28−S51). For **NI-PTZ-1** in CHX, an excited-state absorption (ESA) band centered at 465 nm was observed, together with a lower intensity absorption band centered at 366 nm (Figure 8a). These are the typical ESA bands of the ^{3}NI* state.[63,80,81] Furthermore, a weak ground-state bleaching (GSB) band centered at 330 nm was observed, which is in agreement with the steady-state absorption of the NI moiety. The same ^{3}NI* ESA band has also been observed for the NI-PTZ dyad containing a flexible polymethylene linker (in TOL).[60] The intrinsic triplet-state lifetime of **NI-PTZ-1** was obtained by fitting the experimental curves based on the kinetic model with the TTA self-quenching effect considered and was determined as 274.7 μs by monitoring the decay trace at 470 nm (Figure 8d). This is an interesting result since we observed CS emission for **NI-PTZ-1** when measuring the fluorescence (Figure 4a), and it indicates that since the ^{3}NI* state has lower energy than the CS state, the apparent long CS-state lifetime is due to the energy pooling effect of the lower, dark ^{3}NI* state. The discrepancy between the delayed fluorescence lifetime (321.5 μs, Figure 4a) and the detected ^{3}NI* state lifetime (τ_{int} = 274.7 μs) is probably due to the TTA self-quenching effect in the ns-TA study.

The ns-TA spectra of **NI-Ph** and **NI-PTZ-O** were also studied (Figures S47 and S48, CHX) and similar ESA bands centered at 470 and 360 nm were observed. The triplet-state lifetime of **NI-Ph** was determined as 153.7 μs in N_2-saturated CHX, which is shortened to 445 ns under air atmosphere. Similar results were observed for **NI-PTZ-O** (τ = 191.1 μs in N_2-saturated CHX, τ = 556 ns under air atmosphere). Differently from a recently reported compact NI-PTZ dyad, for which a short-lived CS state (2.6 μs) was observed in ns-TA spectra, for **NI-PTZ-1**, no CS state was observed in CHX.[63]

Similar results were observed for **NI-PTZ-2** and **NI-PTZ-3**: in both cases, ESA bands characteristic for the ^{3}NI* state were observed in the ns-TA spectra (Figures S32, S36, S53, and S54), with intrinsic lifetimes of 193.4 and 180.3 μs, respectively. Under air atmosphere, the triplet-state lifetimes of **NI-PTZ-1**, **NI-PTZ-2**, and **NI-PTZ-3** (in CHX) decreased to 442, 445, and 453 ns, respectively. This is a further evidence that the transient species are localized triplet excited states (^{3}LE state, ^{3}NI*).

Then, we examined the ns-TA spectra of **NI-PTZ-1** in a polar solvent (ACN, $E_T(30)$ = 45.6 kcal mol^{-1}, Figure 8c). Interestingly, a narrow band centered at 412 nm and a broad absorption band centered at 510 nm were observed (Figure 8c). Based on the spectroelectrochemistry and chemical oxidation study (Figures 6 and S61), these absorption bands can be attributed to $NI^{-\bullet}$ and $PTZ^{+\bullet}$, respectively. This result is also in agreement with the previous assignment of the CS state in a NI-PTZ dyad containing a flexible polymethylene linker.[60] The decays of the kinetic traces at both 420 and 520 nm are biexponential (Figures 8f and S28), with a fast decaying component of 1.4 μs (69%) and a slower decaying component with a lifetime of 15.0 μs (31%). The short-lived component is attributed to the intramolecular CR and the long-lived component to the intermolecular CR.[60] This interpretation is confirmed by measuring ns-TA spectra in a highly viscous polar solvent, for instance, diethylene glycol ($E_T(30)$ = 53.8 kcal mol^{-1}, η = 35.7 mPa s, 20 °C) because the diffusion will be inhibited to a large extent in a viscous solvent. In this solvent, the decay traces monitored at 420 and 520 nm are monoexponential with lifetimes of 406 and 420 ns, respectively (Figure S40). These results indicate intermolecular electron transfer for **NI-PTZ-1** in ACN. The quantum yield of the CS state (Φ_{CS}) was determined using a relative method with anthracene as a standard (for details, please refer to the Supporting Information). In ACN, the Φ_{CS} of **NI-PTZ-1**−**3** was determined as 8.6, 7.4, and 7.0%, respectively (Figure S55). It should be noted that the Φ_{CS} in ACN is attributed to the ^{3}CS state due to the long lifetime detected in ns-TA rather than total CS states (both ^{1}CS and ^{3}CS states). The observation of the long-lived CS state (τ_{CS} = 1.4 μs), yet the lack of TADF in ACN, confirms the spin-vibronic coupling mechanism of the TADF.[82−84] It is worth to note that the lifetime in diethylene glycol is insensitive to O_2 (374.3 and 387.2 ns at 420 and 520 nm, respectively, Figure S41), due to the retarded diffusion.[60] Similar results were observed for **NI-PTZ-2** (1.3 μs (59.6%)/11.8 μs (40.4%)) and **NI-PTZ-3** (1.1 μs (59.2%)/19.8 μs (40.8%)) at 420 nm in ACN (Figures S32 and S36).

The CS-state lifetime is longer as compared to some similar dyads. In a triad with PTZ as the electron donor, ethynyl-NI as the electron acceptor, and a trans bis(alkylphosphine) Pt(II) acetylide coordination framework as the chromophore and the linker, the CS-state lifetime is very short (ca. 1 ns).[85] This is interesting because in this triad, the distance between the NI and PTZ moieties is quite large, and the coupling between the donor and the acceptor is weak, which should lead to a long-lived CS state. A longer lifetime of 178 ns was observed in the case of a donor−chromophore−acceptor triad with PTZ as the electron donor, C_{60} as the electron acceptor, and N^N Pt(II) bisacetylide complex as the linker. It was proposed that the electron spin control contributes to a long lifetime; however, the electron spin multiplicity of the CS state was not reported.[26] The CS-state lifetimes of the current compact dyads are even longer than the CS-state lifetimes of dyads with PTZ as the electron donor, pyromellitdiimide as the acceptor, and biphenyl as the linker (0.15 μs).[86]

For the current NI-PTZ dyads, we observed the CS state with a lifetime of 38.2 ns for **NI-PTZ-1** at 520 nm (**NI-PTZ-2**: 47.1 ns; **NI-PTZ-3**: 31.0 ns) in ACN under air atmosphere. It is worth noting that the decay of the transient species monitored at 520 nm is 38.2 ns using a 2000 ns detection window, but it extends to 32.4 μs using a 100 μs detection window (**NI-PTZ-1**, Figure S29). This is an interesting example of a long-lived CS state (1.4 μs) observed in a compact electron donor−acceptor dyad.[3] Comparison with previously reported systems shows that a CS state was observed for a compact electron donor−acceptor dyad with a Zn(II) porphyrin electron donor and pyromellitimide or naphthalenediimide as the electron acceptor (the two units are connected by a single C−N bond), but the CT lifetime is much shorter (2.1−200 ps).[87] A similar observation was made in the case of a rigid electron donor−acceptor dyad with dimethoxy naphthalene as the electron donor and a dimethyl

https://doi.org/10.1021/acs.jpcb.3c02595
J. Phys. Chem. B XXXX, XXX, XXX−XXX

cyclobut-1-ene-1,2-dicarboxylate unit as the electron acceptor (the linker between the two units is norbornane), the ^{1}CS state formed by direct photoexcitation is short-lived (τ < 10 ps), whereas the ^{3}CS state produced by intermolecular triplet photosensitization showed a much longer lifetime of 1.4 μs.[88] Also, in a conjugate of *N,N′*-bis-1,8-naphthalimide and spermine dyad with spermine as the electron donor, a CS state and ^{3}NI* state were observed, with lifetimes of 12 and 4.2 μs, respectively.[89] Note that the CS state of the current compact dyads in ACN have lifetimes of 1.1−1.4 μs, similar to the previously reported NI-PTZ dyads containing flexible linkers.[60] It is significant to observe such long CS lifetimes in compact electron donor−acceptor dyads, considering the strong electronic coupling. The most probable factor contributing to the long CS-state lifetime is the electron spin control effect, i.e., the formation of the ^{3}CS state,[3] as well as the Marcus inverted region effect of the CR process.

It should be noted that for the previously reported NI-PTZ dyads, in which the donor and acceptor are separated by saturated polymethylene linkers, the intramolecular CS state is short-lived (ca. 300 ns).[60] The CS lifetime of **NI-PTZ-1** is similar to that of an anthraquinone−PTZ dyad, presenting a long, saturated bicyclo[2.2.2]octane linker (τ_{CS} = 1.0 μs).[19] Previously, a long-lived CS state was observed for a zinc chlorin−C_{60} dyad (230 μs).[21] This long lifetime was attributed to the lack of the quantum tunneling effect,[77] but the contribution from the small λ of the electron acceptor C_{60} and thus the Marcus inverted region effect of the CR process cannot be excluded.[20] Recently, we have shown that in a spiro rhodamine−NI compact dyad, where we observed a CS state (τ = 0.94 μs), the ^{3}NI* state is the precursor for CS, and the long-lived CS state is in triplet multiplicity.[90] Similar observation has been made for donor−acceptor units linked to a transition-metal coordination framework, where the ^{3}MLCT state is the precursor for CS, and a long-lived ^{3}CS state is formed.[22,24] Thus, we propose that the long CS lifetime of the current compact dyads is due to the electron spin control effect, i.e., the formation of a ^{3}CS state instead of the normally observed SCRP, or the formation of free ion pairs without electron spin−spin interaction.[3,22−24,62,91]

Interestingly, in TOL, the ns-TA spectra of **NI-PTZ-1** (Figures 8b and S28) are neither similar to those observed in CHX nor in ACN. A sharp absorption band centered at 416 nm was observed, together with a broad band centered at 480 nm, with a shoulder beyond 500 nm. Based on our previous studies, these three absorption bands are attributed to $NI^{-\bullet}$, ^{3}NI*, and $PTZ^{+\bullet}$, respectively. Therefore, both the ^{3}NI* and CS states were observed in TOL. This is reasonable, since the polarity of TOL (relative dielectric constant, ε_r = 2.38, $E_T(30)$ = 33.9 kcal mol^{-1}) is between that of CHX (ε_r = 2.0, $E_T(30)$ = 30.9 kcal mol^{-1}) and ACN (ε_r = 35.9, $E_T(30)$ = 45.6 kcal mol^{-1}). The decay of the transient species is multiexponential, with lifetimes of 27 ns (92.4%)/3.5 μs (6.6%)/27.1 μs (1.0%) at 420 nm (Figure 8e). Similar results were observed at 470 nm (36 ns (81.5%)/3.4 μs (12.0%)/43.3 μs (5.5%)) and 520 nm (32 ns (81.5%)/3.4 μs (12.0%)/46.1 μs (6.5%), Figure S28). We tentatively assign the species with a lifetime of 27 ns to the ^{1}CS state, the species with 3.5 μs to the ^{3}CS state, and the lifetime of 27.1 μs to the intermolecular CR. In order to study the excited-state dynamics in detail, the evolution of ns-TA spectra in the early delay time domain was analyzed (Figure S31). The first species has sharp positive bands at 418 and 492 nm, and these bands are assigned to the $NI^{-\bullet}$ species pertaining to the ^{1}CS state. Then, within 33.4 ns, this spectrum evolves to the second component, which has prominent positive bands at 418 and 470 nm, and a minor band at 515 nm. The former are assigned to $NI^{-\bullet}$ and ^{3}NI* and the latter is assigned to $PTZ^{+\bullet}$. Thus, we propose at this timescale that both the ^{3}NI* and ^{3}CS state exist. A ^{1}CS → ^{3}NI* process by spin−orbit charge-transfer intersystem crossing (SOCT-ISC) mechanism for **NI-PTZ-1** takes about 33.4 ns, and ^{3}CS state and ^{3}NI* states are in equilibrium at the long delay time. This slow CS is similar to that observed with a NI-PTZ dyad containing a flexible polymethylene linker (1−3.8 ns).[60] Recently, with a spiro compact electron donor−acceptor dyad, in which the electron donor (closed form of rhodamine) and the electron acceptor (NI moiety) are separated by three σ-bonds, the ^{3}LE → CS takes 125 ns.[81] Furthermore, in TOL, the Φ_{CS} of **NI-PTZ-1−3** were determined as 54.0, 54.8, and 49.7%, respectively.

For the flexible NI-PTZ dyads, similar results were observed in TOL;[60] however, the CS state is short-lived (0.9−2.8 ns), and only the ^{3}NI* state is persistent till 5 ns. Based on the spectral evolution of the flexible NI-PTZ dyads, it is clear that ^{3}NI* and CS states are not in equilibrium.[60] Thus, **NI-PTZ-1** gives drastically different results as compared to the previously reported flexible NI-PTZ dyads. Similar results were observed for **NI-PTZ-2** and **NI-PTZ-3** in TOL upon photoexcitation (Figures S32−S39); however, it was found that the CS state decays faster than the ^{3}NI* state for these two dyads.

3.6. Time-Resolved Electron Paramagnetic Resonance (TREPR) Spectroscopy. The excited states of the dyads were also studied with time-resolved electron paramagnetic spin (TREPR) spectroscopy (Figure 9). First, the reference compound **NI-Ph** was studied (Figure 9a). It is known that NI has ISC ability,[92] but the ISC of **NI-Ph** is poor as confirmed by ultrafast spectroscopy (Tables 1 and S8).[93] Upon pulsed laser excitation in the frozen solution of TOL/2-MeTHF (1/1, v/v) at 80 K, a typical triplet-state TREPR spectrum of organic molecules randomly oriented in a magnetic field was observed, with the electron spin polarization (ESP) phase pattern as (*e*, *e*, *a*, *e*, *a*, *a*) at canonical orientations.[1,94−97] The simulation of the TREPR spectrum gives the zero-field splitting (ZFS) |*D*| and *E* parameters as 2500 and −125 MHz, respectively. These values are very close to the previously reported results 2472 and 135 MHz for the triplet state of native NI.[93] 4-BromoNI shows slightly larger ZFS parameters, with |*D*| and |*E*| as 2590 and 150

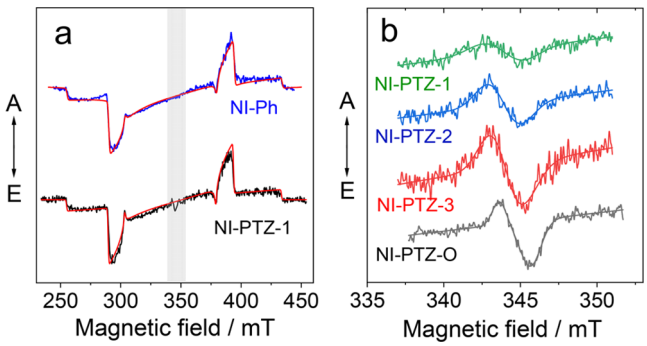

Figure 9. TREPR spectra of (a) **NI-PTZ-1** ($c = 4.0 \times 10^{-4}$ M) and **NI-Ph** ($c = 3.0 \times 10^{-4}$ M) in TOL/2-MeTHF (v/v, 1/1) frozen mixed solution; (b) central part of TREPR spectra of **NI-PTZ-1** ($c = 4.0 \times 10^{-4}$ M), **NI-PTZ-2** ($c = 3.0 \times 10^{-4}$ M), **NI-PTZ-3** ($c = 4.0 \times 10^{-4}$ M), and **NI-PTZ-O** ($c = 1.0 \times 10^{-4}$ M). λ_{ex} = 355 nm, 80 K, delay after flash (DAF) = 500 ns. The fitting parameters are presented in Table 3.

https://doi.org/10.1021/acs.jpcb.3c02595
J. Phys. Chem. B XXXX, XXX, XXX−XXX

MHz, respectively.[63] For 3-bromoNI, the ZFS |D| and |E| are 2750 and 120 MHz, respectively.[98] The population ratio of the three sublevels of the T_1 state (T_X, T_Y, and T_Z) is $P_X/P_Y/P_Z$ = 0:0:1 (unique rates: $\Delta p = |P_X - P_Y|/|P_Y - P_Z| = 0:1$).

The dyads were also studied with TREPR spectroscopy (Figures 9a and S65). **NI-PTZ-1** shows virtually the same TREPR spectrum as that of **NI-Ph**. The ESP phase pattern of the triplet-state TREPR spectrum is (*e*, *e*, *a*, *e*, *a*, *a*), which is different from the previously reported NI-PTZ compact dyads with the PTZ unit connected at the 4-position of the NI moiety.[63] The simulation of the TREPR spectra gives the ZFS |D| and *E* parameters as 2500 and −132 MHz, respectively (Table 3).

Table 3. Zero-Field Splitting Parameters (|D| and *E*) and Relative Populations $P_{X,Y,Z}$ of the Spin States at Zero Magnetic Field of Compounds[a]

	|D| (MHz)	*E* (MHz)	P_X	P_Y	P_Z	*g*-factor
NI-PTZ-1	2500	−132	0.87	0.13	0	2.0025
NI-PTZ-2	2500	−132	0.89	0.11	0	2.0025
NI-PTZ-3	2500	−132	0.90	0.10	0	2.0025
NI-PTZ-O	2500	−132	0.83	0.18	0	2.0030
NI-Ph	2500	−132	0.82	0.18	0	2.0025

[a]Obtained from simulations of the triplet-state TREPR spectra of the indicated molecules at 80 K. P_i is the relative population of the *i*th ZFS state. An isotropic *g*-value of 2.0025 was chosen for the spectral simulations of two molecules.

These values are close to the NI chromophore; therefore, we conclude the triplet state is confined on the NI moiety (i.e., a ^{3}LE state). This is supported by the higher T_1 state energy of the PTZ moiety (2.6 eV) than the NI unit (2.3 eV).[60,99] Moreover, the triplet state of PTZ unit was reported to have a much large ZFS *D* value of 3747 MHz.[100]

Interestingly, simulations show that the population ratio of the three sublevels of the T_1 state (T_X, T_Y, and T_Z) is $P_X/P_Y/P_Z$ = 0.87:0.13:0 ($\Delta p = |P_X - P_Y|/|P_Y - P_Z| = 0.74:0.13$). This ESP phase pattern is similar to that of **NI-Ph**. This result indicates that the triplet state of **NI-PTZ-1** in frozen solution at 80 K occurs via the SOC-ISC, not the SOCT-ISC or other CR-induced ISC processes. This scenario is similar to the NI-anthryl dyads with a phenyl linker between the two units,[93] and is supported by the results observed with the NI-PTZ dyad containing a flexible linker for which it was proposed that ^{1}NI* is the precursor of the CS state, and the ^{3}NI* state was not formed by CR.[60] Note that in frozen solution at 80 K, the solvation effect is eliminated to a large extent; thus, the polarity of the microenvironment should be very low. Similar results were observed for **NI-PTZ-2** and **NI-PTZ-3**.

Careful examination of the TREPR spectra of **NI-PTZ-1** indicates there is weak, narrow signal in the middle of the spectra (Figure 9a). The width of the bands is ca. ∼20 G. We tentatively assign this signal to the CS state, with a weak spin−spin dipolar interaction between the radical anion and the cation.[101,102] Similar results were observed for **NI-PTZ-2** and **NI-PTZ-3** (Figure S65). These results are drastically different from the previously reported compact NI-PTZ dyad with direct connection of the PTZ and NI moieties at the N-position of the PTZ and the 4-position of the NI moiety for which a ^{3}CS state was observed, and the width of the TREPR spectrum is ca. 600 G, with ZFS *D* and *E* parameters 900 and 0 MHz, respectively.[63] For the previously reported NI-PTZ compact dyad, the electron spin−spin interaction is supposed to be stronger than the current dyads because the donor and acceptor are connected with a C−N single bond, and there is some extent of overlap of the spin density surface of the radical anion and cation.[63] For the current dyads such as **NI-PTZ-1**, however, the overlap of the spin density of the radical anion and cation is negligible because of the intervening phenyl linker and the conformation restriction. Narrow signals have low intensity and are superimposed on a wide signal, which distorts their shape. However, the CS-state TREPR spectrum has an ESP phase pattern of A/E, and signal asymmetry is observed, which is most clearly expressed for the **NI-PTZ-O** compound, and probably reflects the presence of net polarization, which is possible for the triplet precursor spin-correlated radical pairs (SCRP) spectra.

Scheme 2. Photophysical Processes of NI-PTZ-1 in Different Solvents[a]

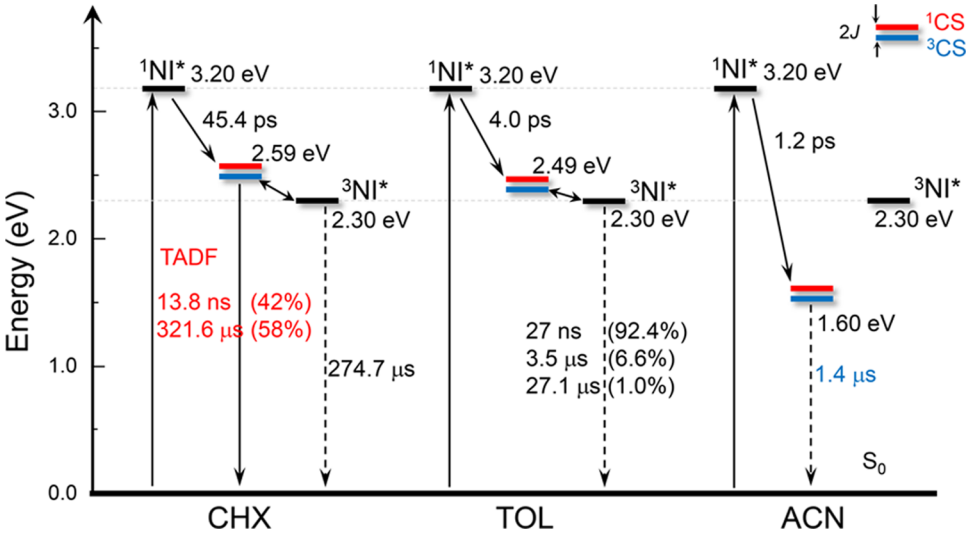

[a]The energy of the excited singlet states is calculated by TDDFT at the B3LYP/6-31G(d) level using Gaussian 09; the energy of CS states is obtained by electrochemical calculation; and the triplet-state energy is estimated by the vibrational 00 transition of $T_1 \rightarrow S_0$ based on phosphorescence spectra. The number of the superscript designates the spin multiplicity.

https://doi.org/10.1021/acs.jpcb.3c02595
J. Phys. Chem. B XXXX, XXX, XXX−XXX

We tentatively attribute this result to the triplet precursor of the CS process to generate ^{3}CS state (i.e., ^{1}NI* ($\rightarrow{}^1$CS) $\rightarrow$ ^{3}NI* $\rightarrow$ ^{3}CS, direct ^{1}CS $\rightarrow$ ^{3}CS is nonefficient).[94,103]

Previously, SCRP was observed for a zinc porphyrin-fullerene dyad (ZnP-C_{60}) bridged by diphenyldisilane at the extended conformation (the distance between the radical anion and cation is 22 Å). The TREPR spectrum of the CS state has A/E polarization pattern, and the width of the spectrum is ca. 30 G.[104] For a zinc chlorin−fullerene compact dyad, a long-lived CS state was observed (lifetime: 230 μs at room temperature), the EPR spectrum of ZnCh-C_{60} in frozen PhCN consists of two characteristic signals, one of which is attributable to an organofullerene radical anion and the other to the zinc chlorin radical cation, but the EPR spectra did not detect a ^{3}CS state (only a sharp signal was observed, with width of ca. 40 G).[21] SCRP and ^{3}CS states were also reported for PTZ−anthraquinone dyads containing a bicyclo[2.2.2]octane linker, for PTZ-B-AQ and PTZ_3-B-AQ, respectively.[89] The TREPR spectrum for PTZ_3-B-AQ at room temperature consisted of four narrow signals (*e*, *a*, *e*, *a*) characteristic of SCRP. The TREPR spectra of current dyads are not detected at room temperature, and spectra of these dyads in frozen solution (Figure 9b) are informative for the evaluation of the spin−spin interaction between the radical anion and cation in the current dyads.

The photophysical properties of **NI-PTZ-1** in different solvents upon photoexcitation can be summarized in Scheme 2. In general, the intervening phenyl linker between the NI and the PTZ moieties makes the CS-state energy higher compared to the recently reported compact NI-PTZ dyad,[63] and thus in CHX, the ^{3}NI* state with the lifetime of 274.7 μs was observed in ns-TA spectra. However, the ^{3}NI* state should have energy very close to the ^{1}CS/^{3}CS states because TADF was observed for **NI-PTZ-1** in CHX. In solvents with slightly higher polarity such as TOL, both ^{3}NI* and CS states were observed. In a polar solvent such as ACN, only the CS state was observed. This is a rare and clear example that the CS-state energy and the order of the CT and the ^{3}LE states can be varied by using solvents with different polarity. In CHX, **NI-PTZ-1** clearly shows TADF, 13.8 ns (42%)/321.6 μs (58%), with a component much larger than the recently reported compact NI-PTZ dyad (22.6 ns (96.6%)/2.6 μs (3.4%)).[63] In TOL, although both the ^{3}CS and ^{3}NI* states were observed in ns-TA spectra, the TADF is not observed. This is a vivid example that an intermediate (energetically closely lying) ^{3}LE state is essential for TADF, probably via the spin-vibronic coupling, to mediate the otherwise nonefficient ^{1}CT $\leftrightarrow$ ^{3}CT interconversion.[51] These results, together with the previously reported analogous dyads, also show that population of the ^{3}CS state alone does not necessarily lead to TADF, and a ^{3}LE state sharing similar energy is necessary for TADF. By detection of the long-lived dark states (CS), we experimentally confirmed the recently proposed spin-vibronic coupling theoretical model of the TADF.

4. CONCLUSIONS

We prepared a series of compact electron donor−acceptor dyads, with naphthalimide (NI) as the electron acceptor and phenothiazine (PTZ) as the electron donor. A phenyl linker is introduced between the donor and acceptor with none, one, or two *ortho*-methyl groups on the linker to impose different steric hindrance and tuning the electronic coupling between NI and PTZ in the dyads. The charge separation (CS), charge recombination (CR), and intersystem crossing (ISC) of the dyads upon photoexcitation were studied with steady-state and time-resolved spectroscopic methods. Interestingly, we observed significant thermally activated delayed fluorescence (TADF) for the dyads, which shows a biexponential decay for the luminescence band centered at 620 nm, i.e., τ = 13.8 ns (population ratio: 42%)/321.6 μs (56%). For the previously reported NI-PTZ dyads containing long and flexible polymethylene linkers, no TADF was observed. TADF has been recently observed for an analogue NI-PTZ compact dyad with a C−N linker, but the luminescence lifetimes are much shorter (22.6 ns/2.6 μs). We found that the prompt fluorescence lifetime is gradually shortened with increasing of the electronic coupling magnitude in the dyads. Most importantly, we observed a long-lived CS state with lifetime up to 1.4 μs (in ACN at room temperature), but no TADF was observed. In CHX, only the ^{3}NI* state was observed (274.7 μs) in nanosecond transient absorption spectra, whereas in TOL, both ^{3}NI* and CS states were observed, which are in good equilibrium (lifetime: 27 ns (92.4%)/3.5 μs (6.6%)/27.1 μs (1.0%)). These results confirm the spin-vibronic coupling mechanism of the TADF, i.e., the intermediate ^{3}LE state is essential for the TADF of electron donor−acceptor dyad emitters. Femtosecond transient absorption spectroscopy indicates that fast CS (1−60 ps) occurs for all of the three dyads in all of the solvents selected, with faster time constants in more polar solvents. Time-resolved electron paramagnetic resonance (TREPR) spectroscopy shows the formation of the ^{3}NI* state in frozen solution at 80 K. A CS state was also observed, with the electron spin−spin interaction magnitude in the middle between that of a spin-correlated radical pair (SCRP) and a ^{3}CS state. Our results are useful for design of compact electron donor−acceptor dyads showing long-lived CS states, and for application of dyads in photocatalysis, photovoltaics, etc.

■ ASSOCIATED CONTENT

Supporting Information

The Supporting Information is available free of charge at https://pubs.acs.org/doi/10.1021/acs.jpcb.3c02595.

General experimental methods, synthesis of compounds, molecular structure characterization, computational details, and additional spectra (PDF)

■ AUTHOR INFORMATION

Corresponding Authors

Jianzhang Zhao − *State Key Laboratory of Fine Chemicals, Frontier Science Center for Smart Materials, School of Chemical Engineering, Dalian University of Technology, Dalian 116024, P. R. China; State Key Laboratory of Chemistry and Utilization of Carbon Based Energy Resources, College of Chemistry, Xinjiang University, Urumqi 830017, P. R. China;* orcid.org/0000-0002-5405-6398; Email: zhaojzh@dlut.edu.cn

Mariangela Di Donato − *LENS (European Laboratory for Non-Linear Spectroscopy), 50019 Sesto Fiorentino (FI), Firenze, Italy; ICCOM-CNR, 50019 Sesto Fiorentino (FI), Italy;* orcid.org/0000-0002-6596-7031; Email: didonato@lens.unifi.it

Violeta K. Voronkova − *Zavoisky Physical-Technical Institute FRC Kazan Scientific Center of RAS, Kazan 420029, Russia*; Email: vio@kfti.knc.ru

https://doi.org/10.1021/acs.jpcb.3c02595
J. Phys. Chem. B XXXX, XXX, XXX−XXX

Authors

Xiao Xiao − *State Key Laboratory of Fine Chemicals, Frontier Science Center for Smart Materials, School of Chemical Engineering, Dalian University of Technology, Dalian 116024, P. R. China*

Yuxin Yan − *State Key Laboratory of Fine Chemicals, Frontier Science Center for Smart Materials, School of Chemical Engineering, Dalian University of Technology, Dalian 116024, P. R. China*

Andrey A. Sukhanov − *Zavoisky Physical-Technical Institute FRC Kazan Scientific Center of RAS, Kazan 420029, Russia*

Sandra Doria − *LENS (European Laboratory for Non-Linear Spectroscopy), 50019 Sesto Fiorentino (FI), Firenze, Italy; ICCOM-CNR, 50019 Sesto Fiorentino (FI), Italy;* orcid.org/0000-0002-9440-1643

Alessandro Iagatti − *LENS (European Laboratory for Non-Linear Spectroscopy), 50019 Sesto Fiorentino (FI), Firenze, Italy; INO-CNR, 50125 Firenze (FI), Italy*

Laura Bussotti − *LENS (European Laboratory for Non-Linear Spectroscopy), 50019 Sesto Fiorentino (FI), Firenze, Italy*

Complete contact information is available at: https://pubs.acs.org/10.1021/acs.jpcb.3c02595

Author Contributions

$^{\nabla}$X.X., Y.Y., A.A.S., and S.D. contributed equally to this work.

Notes

The authors declare no competing financial interest.

■ ACKNOWLEDGMENTS

J.Z. thanks the NSFC (U2001222), the Research and Innovation Team Project of Dalian University of Technology (DUT2022TB10), the Fundamental Research Funds for the Central Universities (DUT22LAB610), and the State Key Laboratory of Fine Chemicals for financial support. A.A.S. and V.K.V. acknowledge financial support from the government assignment for FRC Kazan Scientific Center of RAS. M.D.D. thanks the European Union's Horizon 2020 research and innovation program under Grant Agreement No. 871124, Laserlab, Europe, for the support.

■ REFERENCES

(1) Levanon, H.; Norris, J. R. The Photoexcited Triplet State and Photosynthesis. *Chem. Rev.* **1978**, *78*, 185−198.

(2) Verhoeven, J. W.; van Ramesdonk, H. J.; Groeneveld, M. M.; Benniston, A. C.; Harriman, A. Long-Lived Charge-Transfer States in Compact Donor−Acceptor Dyads. *ChemPhysChem* **2005**, *6*, 2251−2260.

(3) Verhoeven, J. W. On the Role of Spin Correlation in the Formation, Decay, and Detection of Long-Lived, Intramolecular Charge-Transfer States. *J. Photochem. Photobiol., C* **2006**, *7*, 40−60.

(4) Wenger, O. S. Photoinduced Electron and Energy Transfer in Phenylene Oligomers. *Chem. Soc. Rev.* **2011**, *40*, 3538−3550.

(5) Gibbons, D. J.; Farawar, A.; Mazzella, P.; Leroy-Lhez, S.; Williams, R. M. Making Triplets from Photo-Generated Charges: Observations, Mechanisms and Theory. *Photochem. Photobiol. Sci.* **2020**, *19*, 136−158.

(6) Shi, L.; Xia, W. Photoredox Functionalization of C−H Bonds Adjacent to a Nitrogen Atom. *Chem. Soc. Rev.* **2012**, *41*, 7687−7697.

(7) Ravelli, D.; Fagnoni, M.; Albini, A. Photoorganocatalysis. What For? *Chem. Soc. Rev.* **2013**, *42*, 97−113.

(8) De Bonfils, P.; Péault, L.; Nun, P.; Coeffard, V. State of the Art of Bodipy-Based Photocatalysts in Organic Synthesis. *Eur. J. Org. Chem.* **2021**, *2021*, 1809−1824.

(9) Fukuzumi, S. New Development of Photoinduced Electron-Transfer Catalytic Systems. *Pure Appl. Chem.* **2007**, *79*, 981−991.

(10) Wang, Y.; Li, S.; Kershaw, S. V.; Hetsch, F.; Tam, A. Y. Y.; Shan, G.; Susha, A. S.; Ko, C.-C.; Wing-Wah Yam, V.; Yam, V. W.-W.; Lo, K. K. W. Design of a Water-Soluble Hybrid Nanocomposite of CdTe Quantum Dots and an Iridium Complex for Photoinduced Charge Transfer. *ChemPhysChem* **2012**, *13*, 2589−2595.

(11) Suzuki, S.; Matsumoto, Y.; Tsubamoto, M.; Sugimura, R.; Kozaki, M.; Kimoto, K.; Iwamura, M.; Nozaki, K.; Senju, N.; Uragami, C.; et al. Photoinduced Electron Transfer of Platinum(II) Bipyridine Diacetylides Linked by Triphenylamine- and Naphthaleneimide-Derivatives and Their Application to Photoelectric Conversion Systems. *Phys. Chem. Chem. Phys.* **2013**, *15*, 8088−8094.

(12) Song, H.; Zhao, H.; Guo, Y.; Philip, A. M.; Guo, Q.; Hariharan, M.; Xia, A. Distinct Excited-State Dynamics of Near-Orthogonal Perylenimide Dimer: Conformational Planarization versus Symmetry Breaking Charge Transfer. *J. Phys. Chem. C* **2020**, *124*, 237−245.

(13) Xu, Y.; Zheng, J.; Lindner, J. O.; Wen, X.; Jiang, N.; Hu, Z.; Liu, L.; Huang, F.; Würthner, F.; Xie, Z. Consecutive Charging of a Perylene Bisimide Dye by Multistep Low-Energy Solar-Light-Induced Electron Transfer Towards H_2 Evolution. *Angew. Chem., Int. Ed.* **2020**, *59*, 10363−10367.

(14) Ma, Q.; Jia, Z.; Meng, L.; Zhang, J.; Zhang, H.; Huang, W.; Yuan, J.; Gao, F.; Wan, Y.; Zhang, Z.; Li, Y. Promoting Charge Separation Resulting in Ternary Organic Solar Cells Efficiency over 17.5%. *Nano Energy* **2020**, *78*, No. 105272.

(15) Lee, D.; Lee, J.; Sin, D. H.; Han, S. G.; Lee, H.; Choi, W.; Kim, H.; Noh, J.; Mun, J.; Sung, W.; et al. Intrachain Delocalization Effect of Charge Carriers on the Charge-Transfer State Dynamics in Organic Solar Cells. *J. Phys. Chem. C* **2022**, *126*, 3171−3179.

(16) Schuster, D. I.; Cheng, P.; Jarowski, P. D.; Guldi, D. M.; Luo, C.; Echegoyen, L.; Pyo, S.; Holzwarth, A. R.; Braslavsky, S. E.; Williams, R. M.; Klihm, G. Design, Synthesis, and Photophysical Studies of a Porphyrin-Fullerene Dyad with Parachute Topology; Charge Recombination in the Marcus Inverted Region. *J. Am. Chem. Soc.* **2004**, *126*, 7257−7270.

(17) Wiederrecht, G. P.; Svec, W. A.; Wasielewski, M. R.; Galili, T.; Levanon, H. Novel Mechanism for Triplet State Formation in Short Distance Covalently Linked Radical Ion Pairs. *J. Am. Chem. Soc.* **2000**, *122*, 9715−9722.

(18) Dance, Z. E. X.; Mi, Q.; McCamant, D. W.; Ahrens, M. J.; Ratner, M. A.; Wasielewski, M. R. Time-Resolved EPR Studies of Photogenerated Radical Ion Pairs Separated by *p*-Phenylene Oligomers and of Triplet States Resulting from Charge Recombination. *J. Phys. Chem. B* **2006**, *110*, 25163−25173.

(19) Karimata, A.; Kawauchi, H.; Suzuki, S.; Kozaki, M.; Ikeda, N.; Keyaki, K.; Nozaki, K.; Akiyama, K.; Okada, K. Photoinduced Charge Separation of 10-Phenyl-10*H*-Phenothiazine−2-Phenylanthraquinone Dyad Bridged by Bicyclo[2.2.2]octane. *Chem. Lett.* **2013**, *42*, 794−796.

(20) Guldi, D. M. Fullerenes: Three Dimensional Electron Acceptor Materials. *Chem. Commun.* **2000**, 321−327.

(21) Ohkubo, K.; Kotani, H.; Shao, J.; Ou, Z.; Kadish, K. M.; Li, G.; Pandey, R. K.; Fujitsuka, M.; Ito, O.; Imahori, H.; Fukuzumi, S. Production of an Ultra-Long-Lived Charge-Separated State in a Zinc Chlorin−C_{60} Dyad by One-Step Photoinduced Electron Transfer. *Angew. Chem., Int. Ed.* **2004**, *43*, 853−856.

(22) Geiß, B.; Lambert, C. A Small Cationic Donor−Acceptor Iridium Complex with a Long-Lived Charge-Separated State. *Chem. Commun.* **2009**, 1670−1672.

(23) Murakami, M.; Ohkubo, K.; Nanjo, T.; Souma, K.; Suzuki, N.; Fukuzumi, S. Photoinduced Electron Transfer in Photorobust Coumarins Linked with Electron Donors Affording Long Lifetimes of Triplet Charge-Separated States. *ChemPhysChem* **2010**, *11*, 2594−2605.

(24) Hankache, J.; Wenger, O. S. Microsecond Charge Recombination in a Linear Triarylamine−$Ru(bpy)_3^{2+}$−Anthraquinone Triad. *Chem. Commun.* **2011**, *47*, 10145−10147.

(25) Blas-Ferrando, V. M.; Ortiz, J.; Ohkubo, K.; Fukuzumi, S.; Fernández-Lázaro, F.; Sastre-Santos, A. Submillisecond-Lived Photoinduced Charge Separation in a Fully Conjugated Phthalocyanine−Perylenebenzimidazole Dyad. *Chem. Sci.* **2014**, *5*, 4785−4793.

(26) Lee, S.-H.; Chan, C. T.-L.; Wong, K. M.-C.; Lam, W. H.; Kwok, W.-M.; Yam, V. W.-W. Design and Synthesis of Bipyridine Platinum(II) Bisalkynyl Fullerene Donor−Chromophore−Acceptor Triads with Ultrafast Charge Separation. *J. Am. Chem. Soc.* **2014**, *136*, 10041−10052.
(27) Colvin, M. T.; Ricks, A. B.; Scott, A. M.; Smeigh, A. L.; Carmieli, R.; Miura, T.; Wasielewski, M. R. Magnetic Field-Induced Switching of the Radical-Pair Intersystem Crossing Mechanism in a Donor−Bridge−Acceptor Molecule for Artificial Photosynthesis. *J. Am. Chem. Soc.* **2011**, *133*, 1240−1243.
(28) Carmieli, R.; Smeigh, A. L.; Mickley Conron, S. M.; Thazhathveetil, A. K.; Fuki, M.; Kobori, Y.; Lewis, F. D.; Wasielewski, M. R. Structure and Dynamics of Photogenerated Triplet Radical Ion Pairs in DNA Hairpin Conjugates with Anthraquinone End Caps. *J. Am. Chem. Soc.* **2012**, *134*, 11251−11260.
(29) McGarrah, J. E.; Kim, Y.-J.; Hissler, M.; Eisenberg, R. Toward a Molecular Photochemical Device: A Triad for Photoinduced Charge Separation Based on a Platinum Diimine Bis(acetylide) Chromophore. *Inorg. Chem.* **2001**, *40*, 4510−4511.
(30) Chakraborty, S.; Wadas, T. J.; Hester, H.; Schmehl, R.; Eisenberg, R. Platinum Chromophore-Based Systems for Photo-induced Charge Separation: A Molecular Design Approach for Artificial Photosynthesis. *Inorg. Chem.* **2005**, *44*, 6865−6878.
(31) Tao, Y.; Yuan, K.; Chen, T.; Xu, P.; Li, H.; Chen, R.; Zheng, C.; Zhang, L.; Huang, W. Thermally Activated Delayed Fluorescence Materials Towards the Breakthrough of Organoelectronics. *Adv. Mater.* **2014**, *26*, 7931−7958.
(32) Dias, F. B.; Penfold, T. J.; Monkman, A. P. Photophysics of Thermally Activated Delayed Fluorescence Molecules. *Methods Appl. Fluoresc.* **2017**, *5*, No. 012001.
(33) Wex, B.; Kaafarani, B. R. Perspective on Carbazole-Based Organic Compounds as Emitters and Hosts in TADF Applications. *J. Mater. Chem. C* **2017**, *5*, 8622−8653.
(34) Im, Y.; Byun, S. Y.; Kim, J. H.; Lee, D. R.; Oh, C. S.; Yook, K. S.; Lee, J. Y. Recent Progress in High-Efficiency Blue-Light-Emitting Materials for Organic Light-Emitting Diodes. *Adv. Funct. Mater.* **2017**, *27*, No. 1603007.
(35) Cai, X.; Su, S.-J. Marching toward Highly Efficient, Pure-Blue, and Stable Thermally Activated Delayed Fluorescent Organic Light-Emitting Diodes. *Adv. Funct. Mater.* **2018**, *28*, No. 1802558.
(36) dos Santos, P. L.; Etherington, M. K.; Monkman, A. P. Chemical and Conformational Control of the Energy Gaps Involved in the Thermally Activated Delayed Fluorescence Mechanism. *J. Mater. Chem. C* **2018**, *6*, 4842−4853.
(37) Chen, L.; Chen, W.-C.; Yang, Z.; Tan, J.-H.; Ji, S.; Zhang, H.-L.; Huo, Y.; Lee, C.-S. Triplet Harvesting Aryl Carbonyl-Based Luminescent Materials: Progress and Prospective. *J. Mater. Chem. C* **2021**, *9*, 17233−17264.
(38) Li, X.; Shen, S.; Zhang, C.; Liu, M.; Lu, J.; Zhu, L. Small-Molecule Based Thermally Activated Delayed Fluorescence Materials with Dual-Emission Characteristics. *Sci. China: Chem.* **2021**, *64*, 534−546.
(39) Xu, Y.; Xu, P.; Hu, D.; Ma, Y. Recent Progress in Hot Exciton Materials for Organic Light-Emitting Diodes. *Chem. Soc. Rev.* **2021**, *50*, 1030−1069.
(40) Wang, J.; Liang, J.; Xu, Y.; Liang, B.; Wei, J.; Li, C.; Mu, X.; Ye, K.; Wang, Y. Purely Organic Phosphorescence Emitter-Based Efficient Electroluminescence Devices. *J. Phys. Chem. Lett.* **2019**, *10*, 5983−5988.
(41) Bunzmann, N.; Weissenseel, S.; Kudriashova, L.; Gruene, J.; Krugmann, B.; Grazulevicius, J. V.; Sperlich, A.; Dyakonov, V. Optically and Electrically Excited Intermediate Electronic States in Donor:-Acceptor Based OLEDs. *Mater. Horiz.* **2020**, *7*, 1126−1137.
(42) Wang, B.; Zheng, Y.; Wang, T.; Ma, D.; Wang, Q. 1,8-Naphthalimide-Based Hybrids for Efficient Red Thermally Activated Delayed Fluorescence Organic Light-Emitting Diodes. *Org. Electron.* **2021**, *88*, No. 106012.
(43) Peng, J.; Guo, X.; Jiang, X.; Zhao, D.; Ma, Y. Developing Efficient Heavy-Atom-Free Photosensitizers Applicable to TTA Upconversion in Polymer Films. *Chem. Sci.* **2016**, *7*, 1233−1237.
(44) Yanai, N.; Kozue, M.; Amemori, S.; Kabe, R.; Adachi, C.; Kimizuka, N. Increased Vis-to-UV Upconversion Performance by Energy Level Matching between a TADF Donor and High Triplet Energy Acceptors. *J. Mater. Chem. C* **2016**, *4*, 6447−6451.
(45) Yanai, N.; Kimizuka, N. New Triplet Sensitization Routes for Photon Upconversion: Thermally Activated Delayed Fluorescence Molecules, Inorganic Nanocrystals, and Singlet-to-Triplet Absorption. *Acc. Chem. Res.* **2017**, *50*, 2487−2495.
(46) Chen, Q.; Liu, Y.; Guo, X.; Peng, J.; Garakyaraghi, S.; Papa, C. M.; Castellano, F. N.; Zhao, D.; Ma, Y. Energy Transfer Dynamics in Triplet−Triplet Annihilation Upconversion Using a Bichromophoric Heavy-Atom-Free Sensitizer. *J. Phys. Chem. A* **2018**, *122*, 6673−6682.
(47) Zhao, Y.; Wu, Y.; Chen, W.; Zhang, R.; Hong, G.; Tian, J.; Wang, H.; Zheng, D.; Wu, C.; Jiang, X.; et al. The Second Excited Triplet-State Facilitates TADF and Triplet−Triplet Annihilation Photon Upconversion via a Thermally Activated Reverse Internal Conversion. *Adv. Opt. Mater.* **2022**, *10*, No. 2102275.
(48) Ogiwara, T.; Wakikawa, Y.; Ikoma, T. Mechanism of Intersystem Crossing of Thermally Activated Delayed Fluorescence Molecules. *J. Phys. Chem. A* **2015**, *119*, 3415−3418.
(49) Evans, E. W.; Olivier, Y.; Puttisong, Y.; Myers, W. K.; Hele, T. J. H.; Menke, S. M.; Thomas, T. H.; Credgington, D.; Beljonne, D.; Friend, R. H.; Greenham, N. C. Vibrationally Assisted Intersystem Crossing in Benchmark Thermally Activated Delayed Fluorescence Molecules. *J. Phys. Chem. Lett.* **2018**, *9*, 4053−4058.
(50) Noda, H.; Chen, X.-K.; Nakanotani, H.; Hosokai, T.; Miyajima, M.; Notsuka, N.; Kashima, Y.; Brédas, J.-L.; Adachi, C. Critical Role of Intermediate Electronic States for Spin-Flip Processes in Charge-Transfer-Type Organic Molecules with Multiple Donors and Acceptors. *Nat. Mater.* **2019**, *18*, 1084−1090.
(51) Drummond, B. H.; Aizawa, N.; Zhang, Y.; Myers, W. K.; Xiong, Y.; Cooper, M. W.; Barlow, S.; Gu, Q.; Weiss, L. R.; Gillett, A. J.; et al. Electron Spin Resonance Resolves Intermediate Triplet States in Delayed Fluorescence. *Nat. Commun.* **2021**, *12*, No. 4532.
(52) Pearce, N.; Davies, E. S.; Horvath, R.; Pfeiffer, C. R.; Sun, X.-Z.; Lewis, W.; McMaster, J.; George, M. W.; Champness, N. R. Thionated Naphthalene Diimides: Tuneable Chromophores for Applications in Photoactive Dyads. *Phys. Chem. Chem. Phys.* **2018**, *20*, 752−764.
(53) Ge, S.; Li, B.; Meng, X.; Yan, H.; Yang, M.; Dong, B.; Lu, Y. Aggregation-Induced Emission, Multiple Chromisms and Self-Organization of *N*-Substituted-1,8-Naphthalimides. *Dyes Pigm.* **2018**, *148*, 147−153.
(54) Wu, Y.; Chen, X.; Mu, Y.; Yang, Z.; Mao, Z.; Zhao, J.; Yang, Z.; Zhang, Y.; Chi, Z. Two Thermally Stable and AIE Active 1,8-Naphthalimide Derivatives with Red Efficient Thermally Activated Delayed Fluorescence. *Dyes Pigm.* **2019**, *169*, 81−88.
(55) Snellenburg, J. J.; Laptenok, S.; Seger, R.; Mullen, K.; van Stokkum, I. Glotaran: A Java-Based Graphical User Interface for the R Package TIMP. *J. Stat. Software* **2012**, *49*, 1−22.
(56) Sheldrick, G. M. *SADABS, Empirical Absorption Correction Program*; University of Gottingen: Gottingen, Germany, 1996.
(57) Sheldrick, G. M. *SHELXS 97, Program for Crystal Structure Refinement*; University of Gottingen: Gottingen, Germany, 1997.
(58) Sheldrick, G. M. A Short History of SHELX. *Acta Crystallogr., Sect. A: Found. Crystallogr.* **2008**, *64*, 112−122.
(59) Stoll, S.; Schweiger, A. Easyspin, a Comprehensive Software Package for Spectral Simulation and Analysis in EPR. *J. Magn. Reson.* **2006**, *178*, 42−55.
(60) Cho, D. W.; Fujitsuka, M.; Sugimoto, A.; Yoon, U. C.; Mariano, P. S.; Majima, T. Photoinduced Electron Transfer Processes in 1,8-Naphthalimide-Linker-Phenothiazine Dyads. *J. Phys. Chem. B* **2006**, *110*, 11062−11068.
(61) Chen, K.; Yang, W.; Wang, Z.; Iagatti, A.; Bussotti, L.; Foggi, P.; Ji, W.; Zhao, J.; Di Donato, M. Triplet Excited State of Bodipy Accessed by Charge Recombination and Its Application in Triplet−Triplet Annihilation Upconversion. *J. Phys. Chem. A* **2017**, *121*, 7550−7564.
(62) Zhang, X.; Chen, X.; Zhao, J. Electron Spin-Controlled Charge Transfer and the Resulting Long-Lived Charge Transfer State: From

https://doi.org/10.1021/acs.jpcb.3c02595
J. Phys. Chem. B XXXX, XXX, XXX−XXX

Transition Metal Complexes to Organic Compounds. *Dalton Trans.* **2021**, *50*, 59−67.
(63) Tang, G.; Sukhanov, A. A.; Zhao, J.; Yang, W.; Wang, Z.; Liu, Q.; Voronkova, V. K.; Di Donato, M.; Escudero, D.; Jacquemin, D. Red Thermally Activated Delayed Fluorescence and the Intersystem Crossing Mechanisms in Compact Naphthalimide−Phenothiazine Electron Donor/Acceptor Dyads. *J. Phys. Chem. C* **2019**, *123*, 30171−30186.
(64) Cho, D. W.; Fujitsuka, M.; Choi, K. H.; Park, M. J.; Yoon, U. C.; Majima, T. Intramolecular Exciplex and Intermolecular Excimer Formation of 1,8-Naphthalimide−Linker−Phenothiazine Dyads. *J. Phys. Chem. B* **2006**, *110*, 4576−4582.
(65) Verhoeven, J. W.; Scherer, T.; Wegewijs, B.; Hermant, R. M.; Jortner, J.; Bixon, M.; Depaemelaere, S.; de Schryver, F. C. Electronic Coupling in Inter- and Intramolecular Donor-Acceptor Systems as Revealed by Their Solvent-Dependent Charge-Transfer Fluorescence. *Recl. Trav. Chim. Pays-Bas* **1995**, *114*, 443−448.
(66) Gifford, L. A.; Miller, J. N.; Phillipps, D. L.; Burns, D. T.; Bridges, J. W. Phosphorimetric Analysis of Phenothiazine Derivatives. *Anal. Chem.* **1975**, *47*, 1699−1702.
(67) Tang, G.; Yang, W.; Zhao, J. Naphthalimide−Carbazole Compact Electron Donor−Acceptor Dyads: Effect of Molecular Geometry and Electron-Donating Capacity on the Spin-Orbit Charge Transfer Intersystem Crossing. *J. Phys. Chem. A* **2022**, *126*, 3653−3668.
(68) Turro, N. J.; Ramamurthy, V.; Scaiano, J. C. *Principles of Molecular Photochemistry: An Introduction*; University Science Books: Sausalito, 2009.
(69) Ventura, B.; Bertocco, A.; Braga, D.; Catalano, L.; d'Agostino, S.; Grepioni, F.; Taddei, P. Luminescence Properties of 1,8-Naphthalimide Derivatives in Solution, in Their Crystals, and in Co-Crystals: Toward Room-Temperature Phosphorescence from Organic Materials. *J. Phys. Chem. C* **2014**, *118*, 18646−18658.
(70) Valeur, B.; Berberan-Santos, M. *Molecular Fluorescence: Principles and Applications*; Wiley-VCH Verlag GmbH & Co. KGaA: Weinheim, 2012.
(71) Singh-Rachford, T. N.; Castellano, F. N. Photon Upconversion Based on Sensitized Triplet−Triplet Annihilation. *Coord. Chem. Rev.* **2010**, *254*, 2560−2573.
(72) Zhao, J.; Ji, S.; Guo, H. Triplet−Triplet Annihilation Based Upconversion: From Triplet Sensitizers and Triplet Acceptors to Upconversion Quantum Yields. *RSC Adv.* **2011**, *1*, 937−950.
(73) Ye, C.; Zhou, L.; Wang, X.; Liang, Z. Photon Upconversion: From Two-Photon Absorption (TPA) to Triplet−Triplet Annihilation (TTA). *Phys. Chem. Chem. Phys.* **2016**, *18*, 10818−10835.
(74) Guo, X.; Liu, Y.; Chen, Q.; Zhao, D.; Ma, Y. New Bichromophoric Triplet Photosensitizer Designs and Their Application in Triplet−Triplet Annihilation Upconversion. *Adv. Opt. Mater.* **2018**, *6*, No. 1700981.
(75) Rogers, J. E.; Kelly, L. A. Nucleic Acid Oxidation Mediated by Naphthalene and Benzophenone Imide and Diimide Derivatives: Consequences for DNA Redox Chemistry. *J. Am. Chem. Soc.* **1999**, *121*, 3854−3861.
(76) Cho, D. W.; Fujitsuka, M.; Yoon, U. C.; Majima, T. Intermolecular Exciplex Formation and Photoinduced Electron Transfer of 1,8-Naphthalimide Dyads in Methylated Benzenes. *J. Photochem. Photobiol., A* **2007**, *190*, 101−109.
(77) Harriman, A. Unusually Slow Charge Recombination in Molecular Dyads. *Angew. Chem., Int. Ed.* **2004**, *43*, 4985−4987.
(78) Higashino, T.; Yamada, T.; Yamamoto, M.; Furube, A.; Tkachenko, N. V.; Miura, T.; Kobori, Y.; Jono, R.; Yamashita, K.; Imahori, H. Remarkable Dependence of the Final Charge Separation Efficiency on the Donor−Acceptor Interaction in Photoinduced Electron Transfer. *Angew. Chem., Int. Ed.* **2016**, *55*, 629−633.
(79) Zhang, X.; Liu, X.; Taddei, M.; Bussotti, L.; Kurganskii, I.; Li, M.; Jiang, X.; Xing, L.; Ji, S.; Huo, Y.; et al. Red Light-Emitting Thermally-Activated Delayed Fluorescence of Naphthalimide-Phenoxazine Electron Donor-Acceptor Dyad: Time-Resolved Optical and Magnetic Spectroscopic Studies. *Chem.—Eur. J.* **2022**, *28*, No. e202200510.
(80) Samanta, A.; Ramachandram, B.; Saroja, G. An Investigation of the Triplet State Properties of 1,8-Naphthalimide: A Laser Flash Photolysis Study. *J. Photochem. Photobiol., A* **1996**, *101*, 29−32.
(81) Aveline, B. M.; Matsugo, S.; Redmond, R. W. Photochemical Mechanisms Responsible for the Versatile Application of Naphthalimides and Naphthaldiimides in Biological Systems. *J. Am. Chem. Soc.* **1997**, *119*, 11785−11795.
(82) Etherington, M. K.; Gibson, J.; Higginbotham, H. F.; Penfold, T. J.; Monkman, A. P. Revealing the Spin−Vibronic Coupling Mechanism of Thermally Activated Delayed Fluorescence. *Nat. Commun.* **2016**, *7*, No. 13680.
(83) Gibson, J.; Monkman, A. P.; Penfold, T. J. The Importance of Vibronic Coupling for Efficient Reverse Intersystem Crossing in Thermally Activated Delayed Fluorescence Molecules. *ChemPhysChem* **2016**, *17*, 2956−2961.
(84) Kim, I.; Jeon, S. O.; Jeong, D.; Choi, H.; Son, W.-J.; Kim, D.; Rhee, Y. M.; Lee, H. S. Spin−Vibronic Model for Quantitative Prediction of Reverse Intersystem Crossing Rate in Thermally Activated Delayed Fluorescence Systems. *J. Chem. Theory Comput.* **2020**, *16*, 621−632.
(85) Delor, M.; Keane, T.; Scattergood, P. A.; Sazanovich, I. V.; Greetham, G. M.; Towrie, M.; Meijer, A. J. H. M.; Weinstein, J. A. On the Mechanism of Vibrational Control of Light-Induced Charge Transfer in Donor−Bridge−Acceptor Assemblies. *Nat. Chem.* **2015**, *7*, 689−695.
(86) Mori, Y.; Sakaguchi, Y.; Hayashi, H. Spin Chemical Approach Towards Long-Lived Charge-Separated States Generated by Photo-induced Intramolecular Electron Transfer in a Donor−Bridge−Acceptor System. *Bull. Chem. Soc. Jpn.* **2001**, *74*, 293−304.
(87) Yoshida, N.; Ishizuka, T.; Yofu, K.; Murakami, M.; Miyasaka, H.; Okada, T.; Nagata, Y.; Itaya, A.; Cho, H. S.; Kim, D.; Osuka, A. Synthesis of Directly Linked Zinc(II) Porphyrin−Imide Dyads and Energy Gap Dependence of Intramolecular Electron Transfer Reactions. *Chem.—Eur. J.* **2003**, *9*, 2854−2866.
(88) Hviid, L.; Brouwer, A. M.; Paddon-Row, M. N.; Verhoeven, J. W. Long-Lived Short-Distance Intramolecular Charge Separation via Intermolecular Triplet Sensitisation. *ChemPhysChem* **2001**, *2*, 232−235.
(89) Jones, G.; Kumar, S. Participation of Chromophore Pairs in Photoinduced Intramolecular Electron Transfer for a Naphthalimide Spermine Conjugate. *J. Photochem. Photobiol., A* **2003**, *160*, 139−149.
(90) Liu, D.; El-Zohry, A. M.; Taddei, M.; Matt, C.; Bussotti, L.; Wang, Z.; Zhao, J.; Mohammed, O. F.; Di Donato, M.; Weber, S. Long-Lived Charge-Transfer State Induced by Spin-Orbit Charge Transfer Intersystem Crossing (SOCT-ISC) in a Compact Spiro Electron Donor/Acceptor Dyad. *Angew. Chem., Int. Ed.* **2020**, *59*, 11591−11599.
(91) Karimata, A.; Suzuki, S.; Kozaki, M.; Kimoto, K.; Nozaki, K.; Matsushita, H.; Ikeda, N.; Akiyama, K.; Kosumi, D.; Hashimoto, H.; Okada, K. Direct Observation of Hole Shift and Characterization of Spin States in Radical Ion Pairs Generated from Photoinduced Electron Transfer of $(Phenothiazine)_n$−Anthraquinone (n = 1, 3) Dyads. *J. Phys. Chem. A* **2014**, *118*, 11262−11271.
(92) Gerbich, T.; Schmitt, H.-C.; Fischer, I.; Mitrić, R.; Petersen, J. Dynamics of Isolated 1,8-Naphthalimide and *N*-Methyl-1,8-Naphthalimide: An Experimental and Computational Study. *J. Phys. Chem. A* **2016**, *120*, 2089−2095.
(93) Chen, K.; Kurganskii, I. V.; Zhang, X.; Elmali, A.; Zhao, J.; Karatay, A.; Fedin, M. V. Intersystem Crossing and Electron Spin Selectivity in Anthracene-Naphthalimide Compact Electron Donor-Acceptor Dyads Showing Different Geometry and Electronic Coupling Magnitudes. *Chem.—Eur. J.* **2021**, *27*, 7572−7587.
(94) Weber, S. Transient EPR. *eMagRes* **2007**, *6*, 255−270.
(95) Richert, S.; Tait, C. E.; Timmel, C. R. Delocalisation of Photoexcited Triplet States Probed by Transient EPR and Hyperfine Spectroscopy. *J. Magn. Reson.* **2017**, *280*, 103−116.
(96) Hintze, C.; Steiner, U. E.; Drescher, M. Photoexcited Triplet State Kinetics Studied by Electron Paramagnetic Resonance Spectroscopy. *ChemPhysChem* **2017**, *18*, 6−16.

https://doi.org/10.1021/acs.jpcb.3c02595
J. Phys. Chem. B XXXX, XXX, XXX−XXX

(97) Hou, Y.; Zhang, X.; Chen, K.; Liu, D.; Wang, Z.; Liu, Q.; Zhao, J.; Barbon, A. Charge Separation, Charge Recombination, Long-Lived Charge Transfer State Formation and Intersystem Crossing in Organic Electron Donor/Acceptor Dyads. *J. Mater. Chem. C* **2019**, *7*, 12048−12074.
(98) Imran, M.; Sukhanov, A. A.; Maity, P.; Elmali, A.; Zhao, J.; Karatay, A.; Mohammed, O. F.; Voronkova, V. K. Chromophore Orientation-Dependent Photophysical Properties of Pyrene−Naphthalimide Compact Electron Donor−Acceptor Dyads: Electron Transfer and Intersystem Crossing. *J. Phys. Chem. B* **2021**, *125*, 9244−9259.
(99) Bent, D. V.; Hayon, E. Excited State Chemistry of Aromatic Amino Acids and Related Peptides. III. Tryptophan. *J. Am. Chem. Soc.* **1975**, *97*, 2612−2619.
(100) Borowicz, P.; Herbich, J.; Kapturkiewicz, A.; Anulewicz-Ostrowska, R.; Nowacki, J.; Grampp, G. Nature of the Lowest Triplet States of 4′-Substituted *N*-Phenylphenothiazine Derivatives. *Phys. Chem. Chem. Phys.* **2000**, *2*, 4275−4280.
(101) Obondi, C. O.; Lim, G. N.; Churchill, B.; Poddutoori, P. K.; van der Est, A.; D'Souza, F. Modulating the Generation of Long-Lived Charge Separated States Exclusively from the Triplet Excited States in Palladium Porphyrin−Fullerene Conjugates. *Nanoscale* **2016**, *8*, 8333−8344.
(102) Subedi, D. R.; Gobeze, H. B.; Kandrashkin, Y. E.; Poddutoori, P. K.; van der Est, A.; D'Souza, F. Exclusive Triplet Electron Transfer Leading to Long-Lived Radical Ion-Pair Formation in an Electron Rich Platinum Porphyrin Covalently Linked to Fullerene Dyad. *Chem. Commun.* **2020**, *56*, 6058−6061.
(103) Mi, Q.; Ratner, M. A.; Wasielewski, M. R. Time-Resolved EPR Spectra of Spin-Correlated Radical Pairs: Spectral and Kinetic Modulation Resulting from Electron−Nuclear Hyperfine Interactions. *J. Phys. Chem. A* **2010**, *114*, 162−171.
(104) Kobori, Y.; Fuki, M.; Murai, H. Electron Spin Polarization Transfer to the Charge-Separated State from Locally Excited Triplet Configuration: Theory and Its Application to Characterization of Geometry and Electronic Coupling in the Electron Donor−Acceptor System. *J. Phys. Chem. B* **2010**, *114*, 14621−14630.

https://doi.org/10.1021/acs.jpcb.3c02595
J. Phys. Chem. B XXXX, XXX, XXX−XXX